https://doi.org/10.5194/egusphere-2025-376
Preprint. Discussion started: 5 February 2025

A machine learning-based perspective on deep convective clouds and their organisation in 3D. Part II: Spatial-temporal patterns of convective organisation

Sarah Brüning[1] and Holger Tost[1]

[1]Institute for Physics of the Atmosphere, Johannes Gutenberg University Mainz, Johann-Joachim-Becher-Weg 21, Mainz, 55128, Rhineland-Palatinate, Germany

Correspondence: Sarah Brüning (sbruenin@uni-mainz.de)

Abstract. This sequence of papers examines spatio-temporal patterns of convective cloud activity and organisation. In response to the limitations of current remote sensing sensors, our analysis employs a machine learning (ML)-based contiguous 3D extrapolation of 2D satellite data. In Part 2, we investigate spatio-temporal patterns of convective organisation over West Africa and assess their connection to 3D convective cloud and core properties. We employ three organisation indices (COP, SCAI, ROME) to statistically quantify convective organisation. Our results show that convective organisation increases for long-lasting mesoscale cloud systems with numerous deep convective cores. It is likely connected to the Inter-Tropical Convergence Zone (ITCZ) and its northward shift in summer. In spring (March–May), strong convective organisation appears around the Gulf of Guinea and the remote Atlantic Ocean between 15–30° S. The seasonality of convective cloud development induces an increase of the indices between 5–20 % in summer. For instance, the landmass distribution and the influence of extra-tropical dynamics may cause a considerably higher variability in the southern hemisphere. Over the ocean, the organisation indices (COP, SCAI) are about 5–10 % higher than over land. However, derived statistics may be affected by overlapping effects of isolated and clustered convection occurring in the same region. To disentangle their impact calls for an adaptive index. To summarise, combining the information of multiple remote sensing instruments may deliver more profound insights into convective organisation. For future research, we emphasise a further need for a robust quantification of convective organisation.

1 Introduction

Through its contribution to weather and climate variability, atmospheric convection plays an essential role in the climate system (Brune et al., 2020). In the tropics, we observe convective clouds forming as spatially connected structures of extensive size (Houze, 1977). These mesoscale convective systems (MCSs) are one of the main drivers for the transport of heat and moisture through the atmosphere. Furthermore, they enhance the hydrological and radiative variability (Hartmann et al., 1984). MCSs frequently induce severe weather events such as hail and floods (Jin et al., 2022). Recent changes in the large-scale behaviour

https://doi.org/10.5194/egusphere-2025-376
Preprint. Discussion started: 5 February 2025

of convective clouds, notably the degree of spatial clustering (or convective organisation), emphasise MCSs may promote a future increase in precipitation extremes (Becker et al., 2021). However, results for the connection between convective organisation and weather extremes are ambiguous. Tan et al. (2015) express the need for further research on how spatial patterns of convection might change under global warming.

While convective organisation (or aggregation) of deep convection is ubiquitous in the tropics, the underlying mechanisms remain insufficiently understood and may not be well represented in current climate models (Muller and Bony, 2015). An organised state occurs at multiple scales between 100–1000 km and describes how deep convective cells merge into coherent structures such as squall lines, mesoscale convective complexes, or tropical cyclones (Tan et al., 2015; Bläckberg and Singh, 2022). The spatial distribution of convective clouds is not arbitrary. Instead, it is driven by either internal dynamics, like cold pools and radiative feedback, or external forces, such as the land-sea-breeze and other large-scale flows (e.g., Haerter et al. (2019); Coppin and Bony (2015); Dauhut et al. (2016)). Furthermore, aggregation affects the radiative feedback, large-scale circulation, and moisture distribution in the vicinity of a cloud cluster (Hartmann et al., 1984). In an idealised model setup, an aggregated state shows a single region of convective activity surrounded by a drier atmosphere. The feedback between convection, surface fluxes, and radiation further drives aggregation. Former studies agree that the degree of convective aggregation increases with the size and proximity of contiguous convective regions (Tobin et al., 2012). Therefore, an extensive MCS with several regions of convective activity is often associated with stronger convective organisation than isolated convective cells.

Overall, convective organisation is complex to define, in particular when using observational data (Brune et al., 2020). There has yet to be a consensus on quantifying the organisational behaviour of convective clouds (Biagioli and Tompkins, 2023). In response, previous studies have developed various metrics to characterise convective organisation and to provide a deeper understanding about the underlying physical mechanisms (Pscheidt et al., 2019). These indices analyse the spatial distribution of the clouds within a defined area to assess the organisational state. They help differentiate a regularly distributed, randomly distributed, or organised cloud field by using morphological attributes such as the number of clouds, their nearest-neighbour distances, size, shape, pattern, and timing (Pendergrass, 2020; Retsch et al., 2020). So far, the models show convective organisation increases with a warming climate (Wing and Emanuel, 2014). However, there is a lack of evidence about the relationship between aggregation and precipitation extremes (Bläckberg and Singh, 2022). Unlike simulation data, detecting trends of convective aggregation in observational data remains challenging due to the limited extent and quality of historical records and the large variability and low frequency of events most relevant for aggregation (Pendergrass, 2020). In the future, ensuring timely forecasts and a robust climate risk assessment requires even more a correct representation of convective organisation.

Although convective organisation has been the subject of studies using simulation (e.g., Wing et al. (2017); Tompkins and Semie (2017); Rempel et al. (2017)) or observation data (e.g., Tobin et al. (2012); Tan et al. (2015)), we lack an assessment of convective organisation on a regional level. So far, it has been shown that organisation within the tropics can be associated with extreme precipitation (Semie and Bony, 2020). In this study, we aim to provide a deeper understanding of the relationship between cloud properties and convective organisation on a regional scale, comparable to the work of Bao et al. (2024). The area of interest (AOI) covers West Africa and the tropical Atlantic Ocean between 30°N–30° S and 30° W–30° E and lies within the Inter-Tropical Convergence Zone (ITCZ). Here, the environmental conditions favour the development of large clusters of deep

https://doi.org/10.5194/egusphere-2025-376
Preprint. Discussion started: 5 February 2025

convective storm cells (Takahashi et al., 2023). These cells, such as MCSs, affect local weather and contribute 50–90 % of extreme rainfall over continental West Africa (Klein et al., 2021; Atiah et al., 2023; Fink et al., 2006). At the same time, food security and a high climate risk expose West Africa to multiple threats (Berthou et al., 2019). Changing atmospheric conditions could intensify those hazards. Achieving an advanced understanding of convective organisation is crucial to assess the impact of climate change. In the AOI, we find a heterogeneous landmass distribution in the northern and southern hemispheres that controls the development of convection (Brune et al., 2020). Moreover, convective processes differ over land and sea (Zipser et al., 2006). Over the tropical Atlantic Ocean, the large-scale forcing is weaker. As a result, we observe lower cloud tops and less intense rain rates than over continental Africa (Futyan and Genio, 2007). The rainfall variability between the individual regions of the AOI substantially depends on the moisture availability and thermal gradients (Berthou et al., 2019). Overall, the West African monsoon (WAM) dominates the West African climate. A strong temperature gradient between the warm Sahara and the colder waters of the Gulf of Guinea drives the WAM (Fontaine and Philippon, 2000). Stronger convection generally leads to an increase in heavy rain, a larger detrainment, and a slightly smaller thick anvil emissivity. For instance, Stubenrauch et al. (2023) found a distinct annual cycle of convective organisation connected to seasonal shifts of the convective cloud properties.

In Part 1 of this sequence of papers, we derived trajectories of convective clouds and their deep convective core (DCC) regions (Brüning and Tost, 2025). We examined the seasonality of tropical convection and the life-cycle of clustered and isolated convective clouds. In this paper, we aim to complement the findings by including an in-depth analysis of spatio-temporal patterns of convective organisation. We focus on regional and seasonal differences over land and sea within the AOI. In contrast to our former results, we approximate the organisational state not only by the number of DCCs within a cluster (Jones et al., 2024), but we employ organisation indices to quantify convective organisation (Biagioli and Tompkins, 2023). Our study is based on a 4D time series of contiguous 3D radar reflectivities from a machine learning (ML)- based extrapolation of 2D satellite data (Brüning et al., 2024). This novel perspective allows a simultaneous coverage of the horizontal and vertical cloud development over large and remote regions. The results may provide detailed insights on the connection between convective organisation and 3D cloud properties. For the analysis, we employ an object-based algorithm to detect and track convective clouds in the predicted radar reflectivity field. Our aim is to identify how regional patterns of organisation change between seasons, particularly regarding the connection between convective organisation and the spatio-temporal variability of convective cloud development.

We have divided this article into five further sections. In Sect. 2, we describe the data set used in this study. Section 3 presents an overview of metrics employed to quantify convective organisation. Section 4 contains an overview of the results comprising the spatio-temporal variability of organisation indices and cloud microphysical properties. Section 5 discusses the role of the ITCZ and other environmental drivers for the development of large-scale patterns of tropical organisation. Finally, Sect. 6 contains a summary and the main conclusions.

https://doi.org/10.5194/egusphere-2025-376
Preprint. Discussion started: 5 February 2025

2 Data

For this study, we employ contiguous 3D radar reflectivities derived from a ML-based extrapolation of 2D satellite data (Figure 1). In the following section, we provide a brief description of the approach. A more detailed explanation can be found in Brüning et al. (2024). The input data for the ML framework originate from the Spinning Enhanced Visible and Infrared Imager (SEVIRI) sensor onboard the Meteosat-11 (MSG) satellite (Schmetz et al., 2002). We use eight satellite channels and exclude information within the visible spectrum to enable predictions at night (Jones et al., 2023). The ML model is a Res-UNet (Ronneberger et al., 2015) which is primarily trained to reconstruct the 2D vertical cross sections of the radar reflectivity from the Cloud Profiling Radar (CPR) onboard the CloudSat polar-orbiting satellite (Stephens et al., 2008). We apply a spatio-temporal matching algorithm to the MSG SEVIRI channels and the CPR cross sections to extract training samples for our model. The output of the Res-UNet contains not only a reconstruction of the CloudSat cross section, but also an extrapolation of the radar reflectivity to a 3D image, enabling seamless predictions along the whole AOI. We predict the contiguous 3D cloud tomography for each MSG SEVIRI time step of 15 minutes. Based on the native resolution of the MSG SEVIRI images, the data has a spatial resolution of 3 km in the horizontal and 240 m in the vertical dimension.

The 3D radar reflectivities are combined into a 4D time series. Using these data, we track convective clouds and their associated DCCs at each point in time. We define a DCC as a region of high convective activity compared to the cloud anvil. It is characterised by lower temperatures and a strong vertical ascent, which we identify by an extensive vertically contiguous layer and a high radar reflectivity (e.g., Igel et al. (2014); Takahashi et al. (2017)). The workflow for detecting and tracking convective clouds and DCCs follows three steps. At first, we detect convective cloud features by their centroid's position, applying a fixed threshold of -15 dBZ. Then, we use a watershed segmentation algorithm to delineate the associated cloud field for each centroid and split elongated clouds (Sokolowsky et al., 2024). We assign each identified object a unique label to link their movements through time. Then, we apply a second detection framework for each time step to identify DCCs. Our study employs the ML-based radar reflectivity to approximate the convective updraft (Igel et al., 2014). To detect DCCs, we identify a combined local maxima of the radar reflectivity and cloud vertical depth in the 3D cloud field (Feng et al., 2022). Here, the cloud vertical depth describes the difference between the cloud top height (CTH) and cloud base height (CBH) for a vertically contiguous cloud layer (Takahashi et al., 2017). We classify a trajectory as convective when we find at least one DCC, a minimum CTH of 10 km, a maximum CBH of 5 km, and a minimum radar reflectivity of 0 dBZ at 10 km height at least for 15 minutes within the cloud (Chen et al., 2021). A more detailed description of the analysis framework is found in the accompanying paper (Brüning and Tost, 2025).

The AOI is located close to the nadir position of MSG SEVIRI at 0° longitude. Our analysis comprises 6 months of data from March to August 2019, reflecting the northward shift of the ITCZ in West Africa and the onset of the WAM (Kniffka et al., 2019). The detection framework identifies 375,000 trajectories for the period. After filtering the data to exclude clouds with a lifetime of < 1 h, we obtain 300,000 trajectories for analysing the seasonality of convective organisation between spring (March–May, MAM) and summer (June–August, JJA).

https://doi.org/10.5194/egusphere-2025-376
Preprint. Discussion started: 5 February 2025

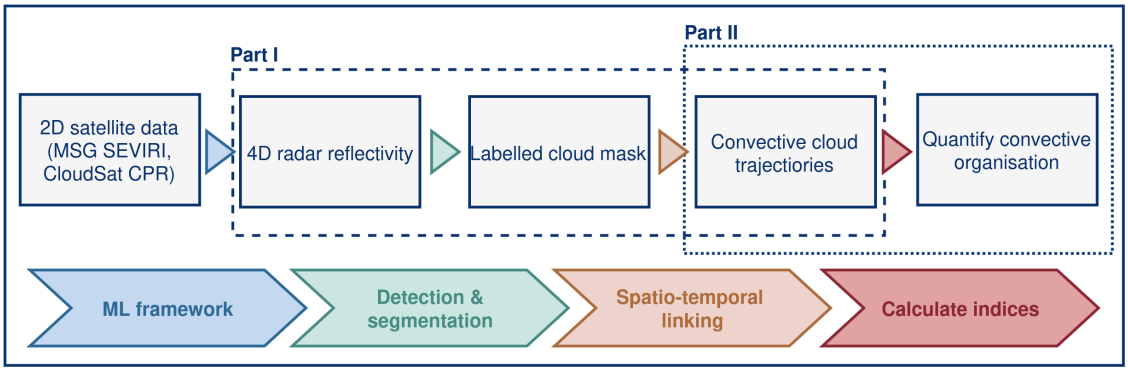

Figure 1. Overview of the workflow to investigate convective organisation using observational data. The study employs 4D radar reflectivities originating a ML-based extrapolation of 2D satellite data. In Part 1 of this sequence of papers, we detect convective clouds within the predicted radar reflectivities and link them through time to create continuous cloud trajectories. In Part 2, these trajectories are used to quantify convective organisation by calculating organisation indices.

3 Method

3.1 Quantifying convective organisation

Convective organisation describes the contrast between convective cells randomly distributed in space and time from those clustering together in an organised state (Pendergrass, 2020). While there exist various organisation indices to quantify the degree of clustering (Biagioli and Tompkins, 2023), each index alone cannot sufficiently characterise convective organisation (Stubenrauch et al., 2023). Instead, all indices have specific limitations, such as a sensitivity to the mean cloud area or to the number of individual objects. In response, we chose a combination of three organisation indices (Mandorli and Stubenrauch, 2024). The input for all indices is a binary field representing the location of labelled convective objects (Semie and Bony, 2020). These cloud labels originate from the convective trajectories described in Sect. 2.

The first index is the simple-to-compute and straightforward Simple Convective Aggregation Index (SCAI). SCAI describes the ratio of the degree of convective disaggregation to a potential maximal disaggregation within a domain (Tobin et al., 2012). The index is unitless and inversely proportional to the number of grid boxes. SCAI compares the number of objects in the domain (N) and the geometric mean distance (D_0) between the centroid positions of all possible object pairs to the possible maximum number of objects that can exist in the domain (N_{max}) and the characteristic domain size (L).

$$\mathrm{SCAI} = \frac{N D_0}{N_{max} L} 1000. \tag{1}$$

SCAI is a unitless index between 0 and infinity whereas lower values point towards a stronger convective organisation. By design, calculating SCAI requires the presence of multiple cloud clusters (Semie and Bony, 2020). It is insensitive to the size of the objects and mainly dominated by the variability in N (White et al., 2018). However, it is less affected by shifts in time and space compared to other indices (Mandorli and Stubenrauch, 2024).

https://doi.org/10.5194/egusphere-2025-376
Preprint. Discussion started: 5 February 2025

The Convective Organization Potential (COP) was developed by White et al. (2018) to overcome some limitations of SCAI. It assumes objects that are larger and closer together are more likely to interact with each other. In contrast to SCAI, the index takes the cloud size into account. COP uses the number of objects (N), the area of the i-th object (A_i), and the distance between the centroids of the i-th and the j-th object (d_{ij}). It adds the characteristic domain size (L) and the total image size (L_2). The index is defined by

$$\mathrm{COP} = \frac{2}{N(N-1)} \sum_{i=1}^{N} \sum_{j=i+1}^{N} \frac{\sqrt{A_i/\pi} + \sqrt{A_j/\pi}}{d_{ij}} \tag{2}$$

which is the mean over all the possible pairs of the interaction potential. COP is a positive and unitless index between 0–1 whereas higher values indicate a stronger convective organisation. Larger and closer objects have a higher increase in COP than small and widespread objects (Pscheidt et al., 2019). While the index correctly increases with the proximity and size, it is sensitive to noise caused in a domain with only a few objects (Mandorli and Stubenrauch, 2024).

SCAI and COP can only be computed when multiple objects are present. In response, we add the Radar Organisation MEtric (ROME) to our analysis. The index considers the average size, proximity, and size distribution of contiguous convective regions (Retsch et al., 2020). Initially, it was designed to analyse radar observations. However, it also worked well with other data (Bläckberg and Singh, 2022). The index assesses connections between pairs of continuous convective regions and assigns a weight to each pair that increases with their respective areas and decreases with their separation distance. The weight is equal to the area of the larger contiguous convective region plus a contribution from the smaller contiguous convective region that depends on the separation distance (Retsch et al., 2020). It employs the smallest distance between the edges of the i-th and the j-th object in the domain ($\tilde{d}_{ij}$) to define

$$\mathrm{ROME} = \frac{2}{N(N-1)} \sum_{i=1}^{N} \sum_{j=i+1}^{N} \cdot \left[A_{ij}^{(max)} + A_{ij}^{(min)} \cdot min\left(1, \frac{A_{ij}^{(min)}}{\tilde{d}_{ij}^2}\right)\right] \tag{3}$$

where $A_{ij}^{(max)} = \max(A_i, A_j)$ and $A_{ij}^{(min)} = \min(A_i, A_j)$. ROME is a positive index measured in units of area. Its value consists of a contribution from the mean area of contiguous convective regions and the distribution of sizes and interaction between different contiguous convective regions. The index is positive, with an increasing ROME value corresponding to a higher degree of aggregation. While ROME is noise-safe and independent of the dataset resolution, it strongly connects to the object size (Biagioli and Tompkins, 2023).

3.2 Grid-based calculation of organisation indices

Convective organisation occurs on a wide range of scales which are generally larger than 100 km (Bläckberg and Singh, 2022). We can calculate the indices for a whole domain to assess the overall strength of convective organisation. However, investigating regional variability demands a further partitioning of the AOI (Figure 2). For this purpose, we use a grid-based approach and divide the AOI into grid cells with a size of 3° (Semie and Bony, 2020). For instance, further studies applied a varying grid cell size between 1° (Jin et al., 2022) and 10° (Tobin et al., 2012) to account for the organisational behaviour of convective clouds. As stated before by Mandorli and Stubenrauch (2024), the number and size of convective clouds highly

https://doi.org/10.5194/egusphere-2025-376
Preprint. Discussion started: 5 February 2025

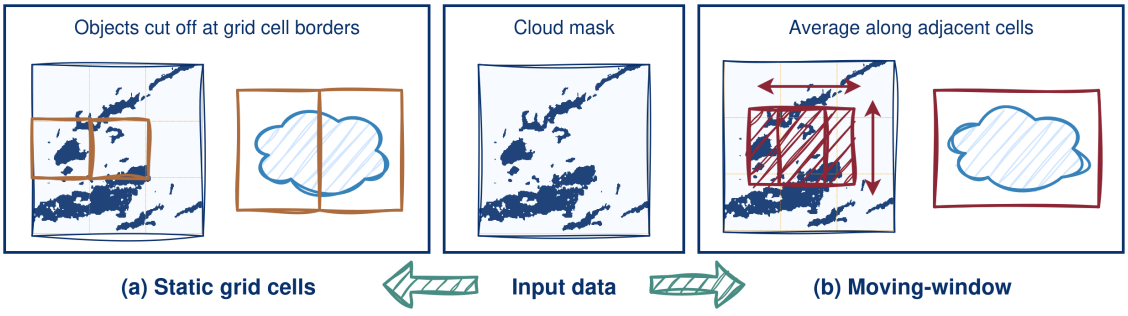

Figure 2. Visualisation of the moving-window approach used to calculate the organisation indices for the labelled cloud mask. For static grid cells **(a)**, clouds may be split at the grid cell borders leading to an enhanced small-scale value variability between grid cells. In this study, we employ a moving-window which iterates along the grid cells **(b)**. In contrast to **(a)**, the indices are less influenced by a single grid cell and rather represent the average composed of all window locations.

affect the organisation indices. Choosing an arbitrary grid cell size and location may cut off contiguous clouds, thus affecting the index. That is why we employ a moving window with a kernel size of 1° x 1° to improve the robustness of our results (Jin et al., 2022). Afterwards, we calculate the three organisation indices (SCAI, COP, and ROME) for every time step.

4 Results

4.1 Characteristics of organisation indices in the tropics

In the following section, we analyse the distribution of the three organisation indices (COP, SCAI, ROME) to derive spatio-temporal patterns of convective organisation over the AOI. By design, COP and ROME behave anti-proportionally to the values of SCAI (White et al., 2018). However, the frequency distribution shows an overlap of lower index values for all indices (Figure 3). In Part 1 of this study (Brüning and Tost, 2025), we found clouds develop about 10 % more frequently over the ocean. This land-sea imbalance is reflected within the frequency distribution of the organisation indices. Most values lie within the lower half of the index scale, either between 0–0.4 for COP and SCAI or between 0–10 000 for ROM. Over land, values are higher in relative terms, in particular for ROME. The results are partly ambiguous as COP and ROME emphasise, on average, a weaker organisation than SCAI.

In Fig. 4, we analyse the distribution of the organisation indices grouped by the surface type. We focus on the diurnal cycle (a–c), zonal changes between 30° S and 30° N (d–f), and the relation between each index and the number of DCCs (g–i). Although we observe differences over land and sea, they account for only up to 10 % of the respective index scale. The diurnal cycle for SCAI is opposed to COP and ROME. All indices indicate the strongest convective organisation in the late evening and early morning hours and the weakest organisation in the afternoon (Figure 4, a–c). The behaviour contradicts the diurnal cycle of cloud formation processes, which show a maximum in the afternoon (land) or late evening (sea) (Cui et al., 2021). In accordance to convective cloud properties, the diurnal differences are lower over the sea than land. The zonal statistics show

https://doi.org/10.5194/egusphere-2025-376
Preprint. Discussion started: 5 February 2025

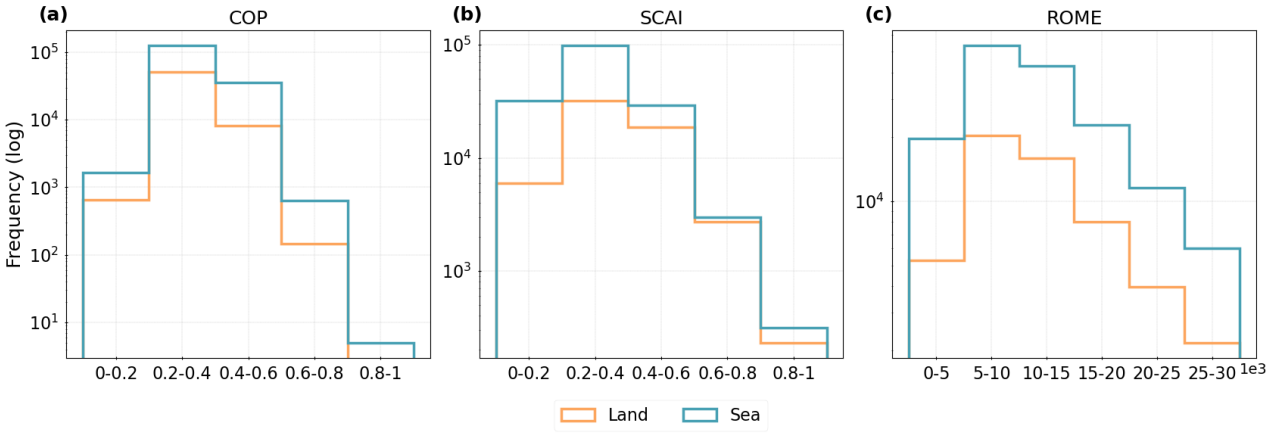

Figure 3. Distribution of convective organisation indices grouped by the surface type. We see the frequencies of **(a)** the COP, **(b)** the SCAI, and **(c)** the ROME on a logarithmic scale.

the weakest convective organisation near the equator and an increase towards the tropics of Cancer and Capricorn (Figure 4, d–f). The highest values of COP and ROME can be found between 10–25° N and S. The value variability is higher over the ocean of the southern hemisphere and land in the northern hemisphere. For SCAI, we observe the lowest values over land between 20–30° N and the ocean between 15–25° S. All three indices point towards a stronger convective organisation with an increasing number of DCCs (Figure 4, g–h). COP and SCAI show a higher organisation over the ocean, whereas ROME is higher over land. The indices' calculation may induce this deviation. In contrast to COP, we can compute ROME when only one labelled cloud is present (Retsch et al., 2020). As a result, a domain with one extensive MCS may have a high ROME but no value for COP and SCAI (Biagioli and Tompkins, 2023).

4.2 Assessing the relation between cloud properties and convective organisation

4.2.1 Patterns of convective cloud development

In Fig. 5, we compute a spatial density distribution for the number of DCCs associated with a convective cloud and plot the locations in spring (MAM) and summer (JJA). In spring (MAM), we observe the highest proportion of isolated convective cells primarily over the Guinea-Congo rainforest and secondarily over the West African coastline (Figure 5, a). Clouds with 2–9 DCCs have a peak occurrence between coastal West Africa and the Gulf of Guinea, whereas highly clustered systems predominantly develop over the Atlantic Ocean between 15–30° W and parts of the tropical rainforest (Figure 5, b–c). In summer (JJA), the ITCZ shifts to its most northward extent (Kniffka et al., 2019). It induces extensive heating in the Sahel, leading to increased land surface temperature anomalies and a higher frequency of deeper convection (Taylor et al., 2022). The hotspot location of isolated convective clouds shifts towards the West African plains and the rainforest north of Congo (Figure 5, d). Custered systems occur more frequently further away from the Atlantic Ocean and up to the Sahel region (Figure 5, e).

https://doi.org/10.5194/egusphere-2025-376
Preprint. Discussion started: 5 February 2025

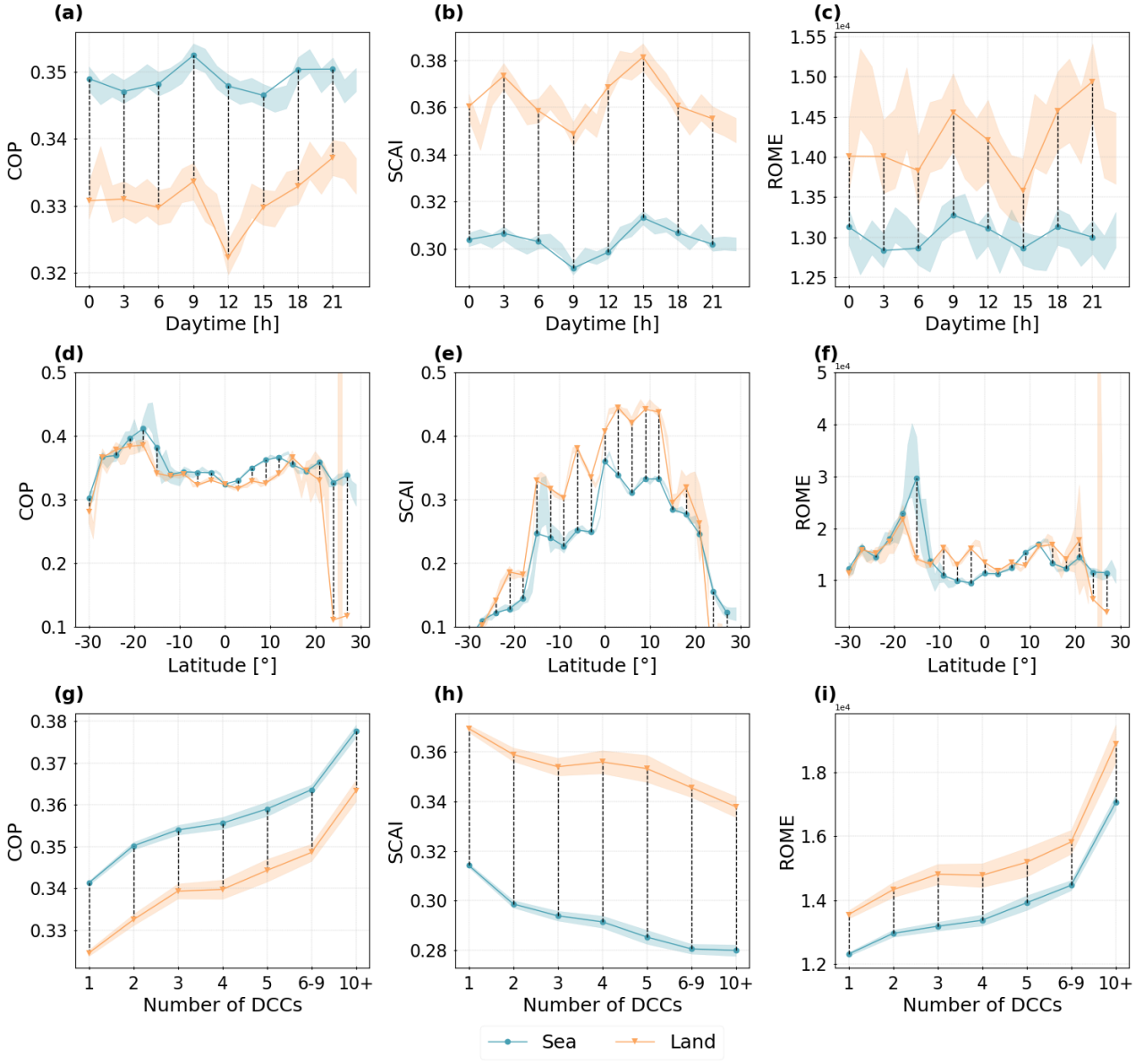

Figure 4. Comparison of the organisation indices behaviour depending on the surface type for **(a)–(c)** the diurnal cycle, **(d)–(f)** the zonal mean, and **(g)–(i)** the number of DCCs for the COP, SCAI, and ROME. Line plots show the mean value with a confidence interval of 95%, black dashed lines refer to the differences over land and sea.

https://doi.org/10.5194/egusphere-2025-376
Preprint. Discussion started: 5 February 2025

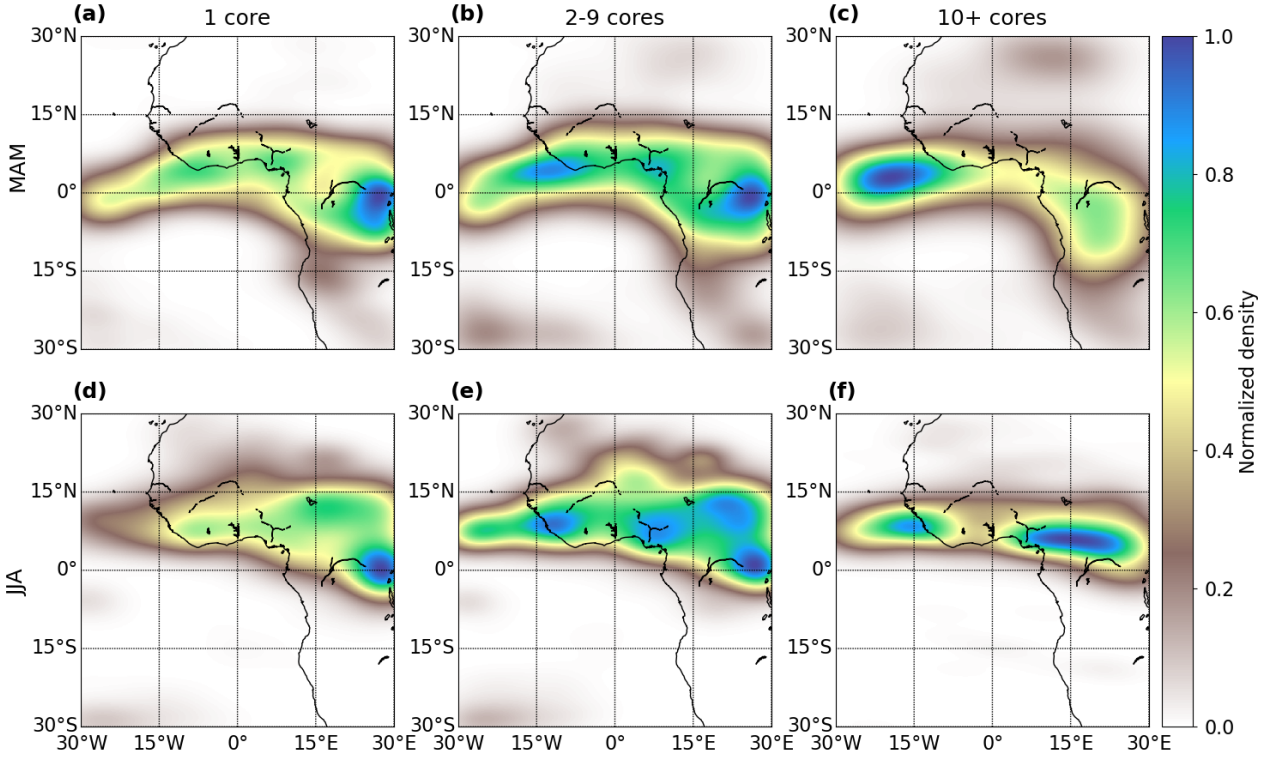

Figure 5. Spatial distribution of clouds grouped by the number of associated cores for spring (MAM, upper row) and summer (JJA, lower row). Clouds are grouped as having **(a) & (d)** a single core, **(b) & (e)** 2-9 cores, and **(c) & (f)** 10 and more cores. The values represent the normalized density for each distribution.

The most highly clustered clouds are confined to two peak regions over the Atlantic Ocean close to the coast of Liberia and between the Jos Plateau and the Cameroon mountains (Figure 5, f).

In a second step, we group the convective clouds by their anvil size to visualise their spatial distribution. We differ three classes for clouds with an anvil smaller than the population's mean size ($\geq$ 1 000 km^2), anvils between the mean and 10 times the mean ($\geq$ 10 000 km^2), and a third, larger, class. Again, the seasonal variations resemble the northward shift of the ITCZ (Figure 5). In spring (MAM), small and medium-sized clouds have a peak occurrence around the equator with a higher spread towards the Gulf of Guinea for medium-sized clouds (Figure 6, a–b). Large clouds show higher seasonal variations. We observe a peak in the southern hemisphere over continental Africa (MAM) (Figure 6, c). In summer (JJA), these former peak regions vanish. The development of MCSs may be affected by alterations of the soil moisture-precipitation feedback or the advection of moist air masses through strong wind shear and convective instability (Nicholson, 2018). Due to the influence of the ITCZ, we see two peaks in the northern hemisphere around the Senegal River and Lake Chad (Figure 6, f). The primary occurrence for small and medium-sized clouds shifts from 5° S–10° N to 5°–20° N (Figure 6, d–e). We generally find highly clustered clouds to be accompanied by a larger cloud anvil size and vice versa (Figure 5,6).

https://doi.org/10.5194/egusphere-2025-376
Preprint. Discussion started: 5 February 2025

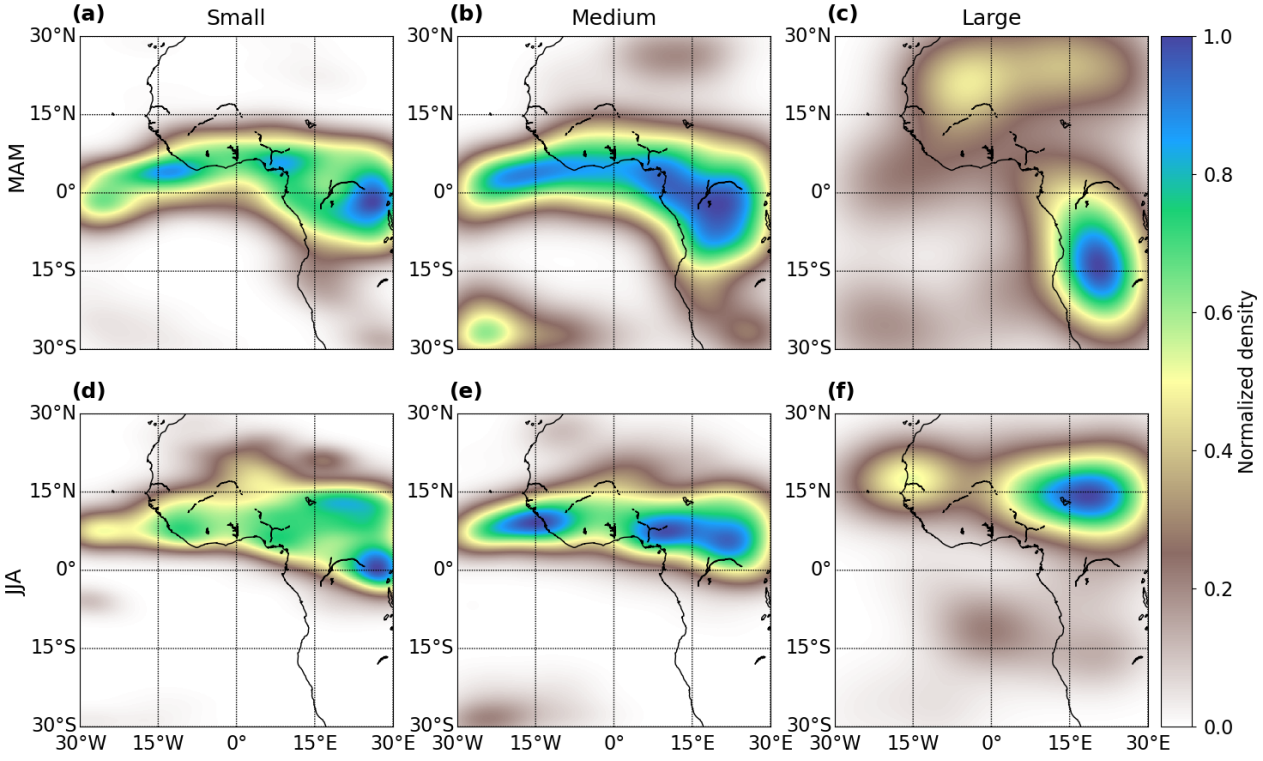

Figure 6. Spatial distribution of clouds grouped by their anvil area for spring (MAM, upper row) and summer (JJA, lower row). Clouds are grouped as **(a) & (d)** small with an anvil area < 1 000 km^2, **(b) & (e)** medium with an anvil area between 1 000–10 000 km^2, and **(c) & (f)** large with an anvil area > 10 000 km^2. The values represent the normalized density for each distribution.

The spatial distribution of the cloud and core properties provides information on regional patterns of convective activity in the AOI (Figure 7). Near the equator, we find smaller cloud anvils, higher cloud tops, a reduced cloud lifetime, an enhanced area ratio, and slightly fewer and smaller DCCs. These properties are typical for fast-evolving, isolated convective cells, which frequently occur between 15° S–15° N (Feng et al., 2022). In contrast, clouds with a large anvil come along a lower CTH, higher cloud lifetime, and a higher number of cores. They appear particularly north of 25° N and south of 15° S. We observe extensive patches of large and long-lived convective cells over the Atlantic Ocean (5–20° S) and the Sahel region (Futyan and Genio, 2007). In the same region, we detect a diverging convective activity regarding the number and size of DCCs. South of 20° S, we find the largest DCCs. However, these convective systems are connected to fewer DCCs, smaller anvils, a lower CTH, and a lower cloud lifetime. In the southern hemisphere, the oceanic circulation and adjacent landmasses may contribute to the development of long-lasting clouds in the Atlantic Ocean (Atiah et al., 2023). Our analysis shows a higher variability between the hemisphere and latitude than for the surface type. Moreover, we detect distinct differences between regions closer to the equator and the tropics.

https://doi.org/10.5194/egusphere-2025-376
Preprint. Discussion started: 5 February 2025

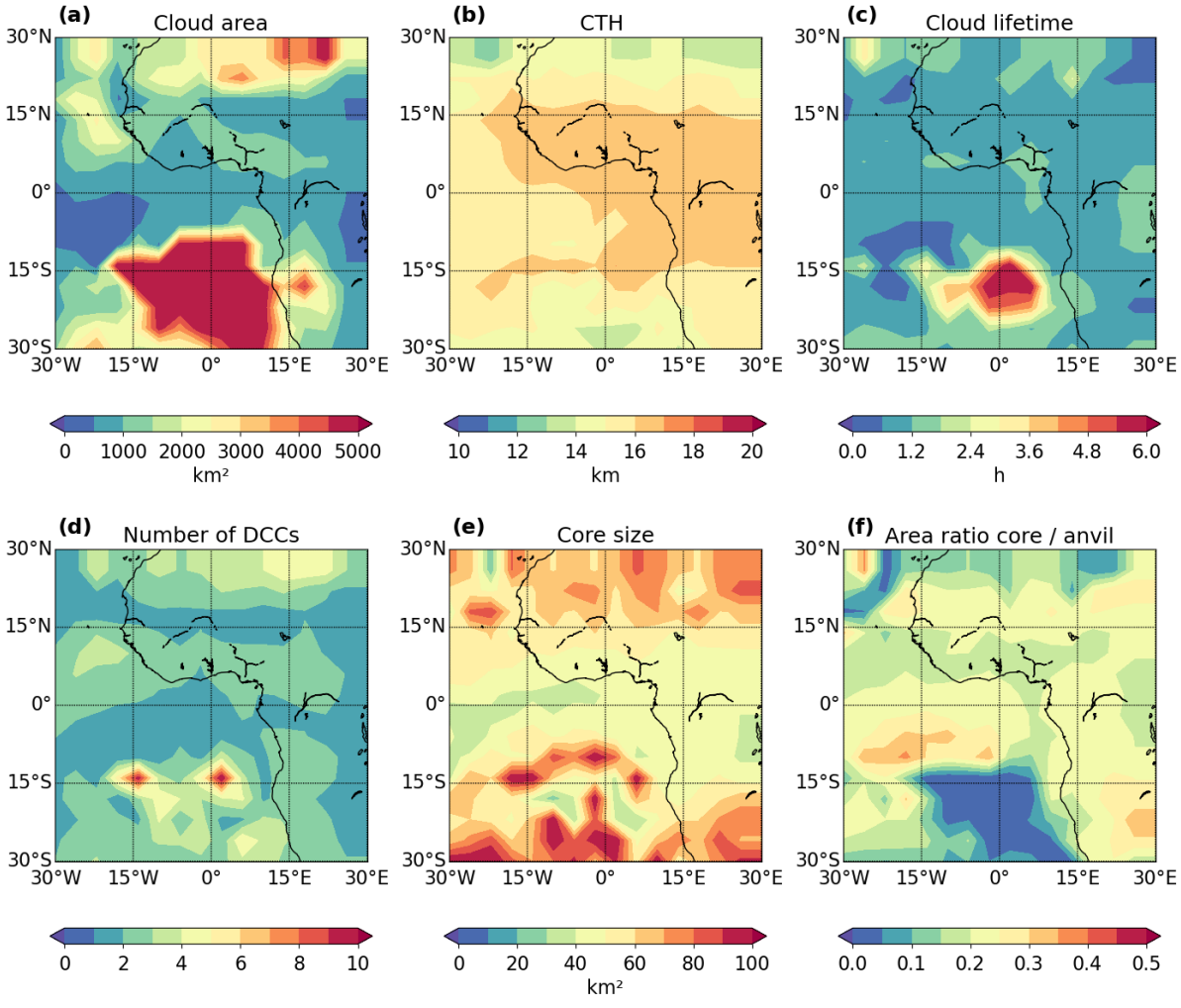

Figure 7. Mean values for cloud and core properties in the AOI interpolated on a 3° x 3° grid. We see **(a)** the cloud anvil area, **(b)** the CTH, **(c)** the cloud lifetime, **(d)** the number of DCCs, **(e)** the convective core size, and **(f)** the area ratio between core and anvil.

https://doi.org/10.5194/egusphere-2025-376
Preprint. Discussion started: 5 February 2025

We extend the analysis by investigating seasonal differences of cloud and core statistics in spring (MAM) and summer (JJA). Figure 8 emphasises that the seasonality of the convective activity depends on the hemisphere. The cloud area is larger in spring over northern Africa (> 15° N) and in summer over West Africa and the Atlantic Ocean (< 15° N). We observe an extensive patch of large cloud anvils in the southern hemisphere that grows in summer. At the same time, the cloud anvil area increases in regions near the equator. Compared to regions near the tropics, equator-near regions show a lower average and variability in the seasonal cycle (Figure 8, a). The CTH in summer is higher over the Atlantic Ocean and the Sahel and lower over coastal West Africa. During this season, we see more DCCs, a larger core size, and a reduced area ratio. With some small-scale deviations, convective activity near the equator increases in summer. We find more clustered clouds and intense convection in spring near the tropic of Cancer. In contrast, convective activity near the tropic of Capricorn is higher in summer. Overall, a higher convective activity comes with a lower area ratio, a higher number of DCCs, a larger cloud and core area, and a longer cloud lifetime. However, local circulations and the landmass distribution may considerably alter the development of convective cells (Atiah et al., 2023).

4.2.2 Identifying regional hotspots of convective organisation

In this section, we analyse the spread of the distribution for each organisation index to identify geographical hotspots of convective organisation. For each index, we calculate the 10th (P10, n = 30 243) and 90th (P90, n = 29 365) percentile as well as the inter-quartile range (IQR) between the 25th and 75th percentile. A hotspot is classified by using the highest (COP, ROME) or lowest (SCAI) 10 % of the data (Semie and Bony, 2020). The IQR of the indices' distribution corresponds to a more random organisation of the clouds.

Section 4.1 shows that the convective organisation is overall weaker around the equator. In this region, we find a high proportion of isolated and short-lived clouds (Section 4.2.1). Their impact on large-scale patterns of organisation is limited compared to MCSs (Takahashi et al., 2023). In our study, the locations of clustered clouds (Figure 5) indicate that clouds with multiple regions of convective activity can be found over land and sea, especially during the summer. At that time, the number and size of DCCs increases, in particular around the equator (Section 4.2.1). The percentiles of the organisation indices correspond predominately to locations around the equator and over the Atlantic Ocean in the southern hemisphere. Around the tropics, we find extensive MCSs and high values for COP and ROME. However, the percentiles show that these locations are considerably affected by outliers. The location of the IQR comprises a band spanning between 10° N–10° S (Figure 9, 10). Within that region, we find more randomly distributed convective cells. The band covers the Atlantic Ocean up to the coastal regions between the Senegal and Ivory Coast (Figure 9, a-b,g-h,i-j). In spring (MAM), this area reaches up to the Congo rainforest at around 12° S, whereas it shifts northward in summer (JJA) (Figure 7). The least organised clouds (P10 COP/ROME, P90 SCAI) appear over the Atlantic Ocean (5° S–5° N) and the rainforest (15°–30° E). In contrast, most organised clouds (P90 COP/ROME, P10 SCAI) occur around the Gulf of Guinea, coastal West Africa and the Atlantic Ocean (> 15° S) (Figure 9). In summer, we see a maximum around the Cameroon mountains and the coastal regions around Senegal up to the Nigerian Planes (Figure 10).

https://doi.org/10.5194/egusphere-2025-376
Preprint. Discussion started: 5 February 2025

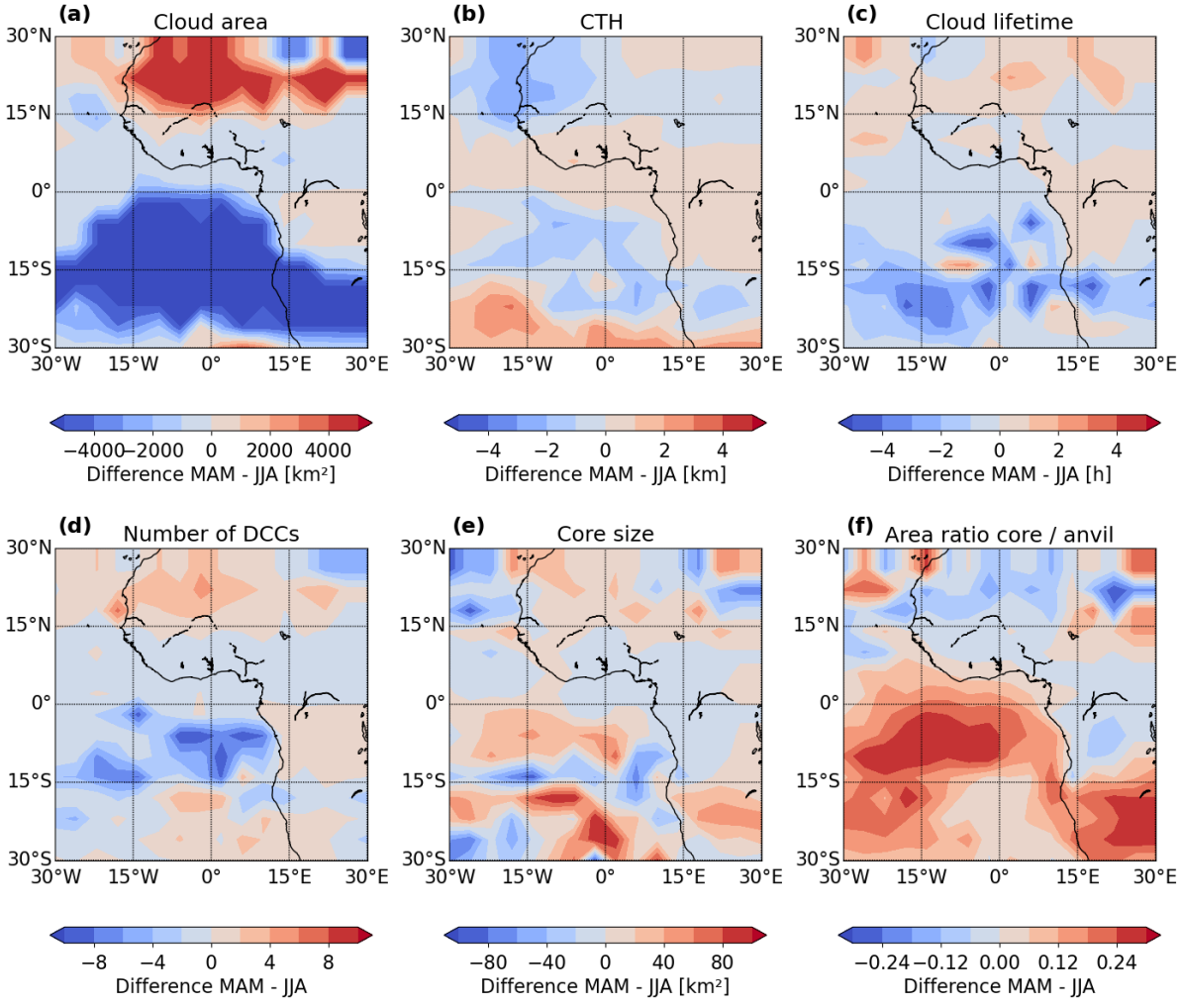

Figure 8. Seasonal differences for cloud statistics in the AOI interpolated on a 3° x 3° grid. We see the difference between spring (MAM) and summer (JJA) season for **(a)** the cloud anvil area, **(b)** the CTH, **(c)** the cloud lifetime, **(d)** the number of DCCs, **(e)** the convective core size, and **(f)** the area ratio between core and anvil.

https://doi.org/10.5194/egusphere-2025-376
Preprint. Discussion started: 5 February 2025

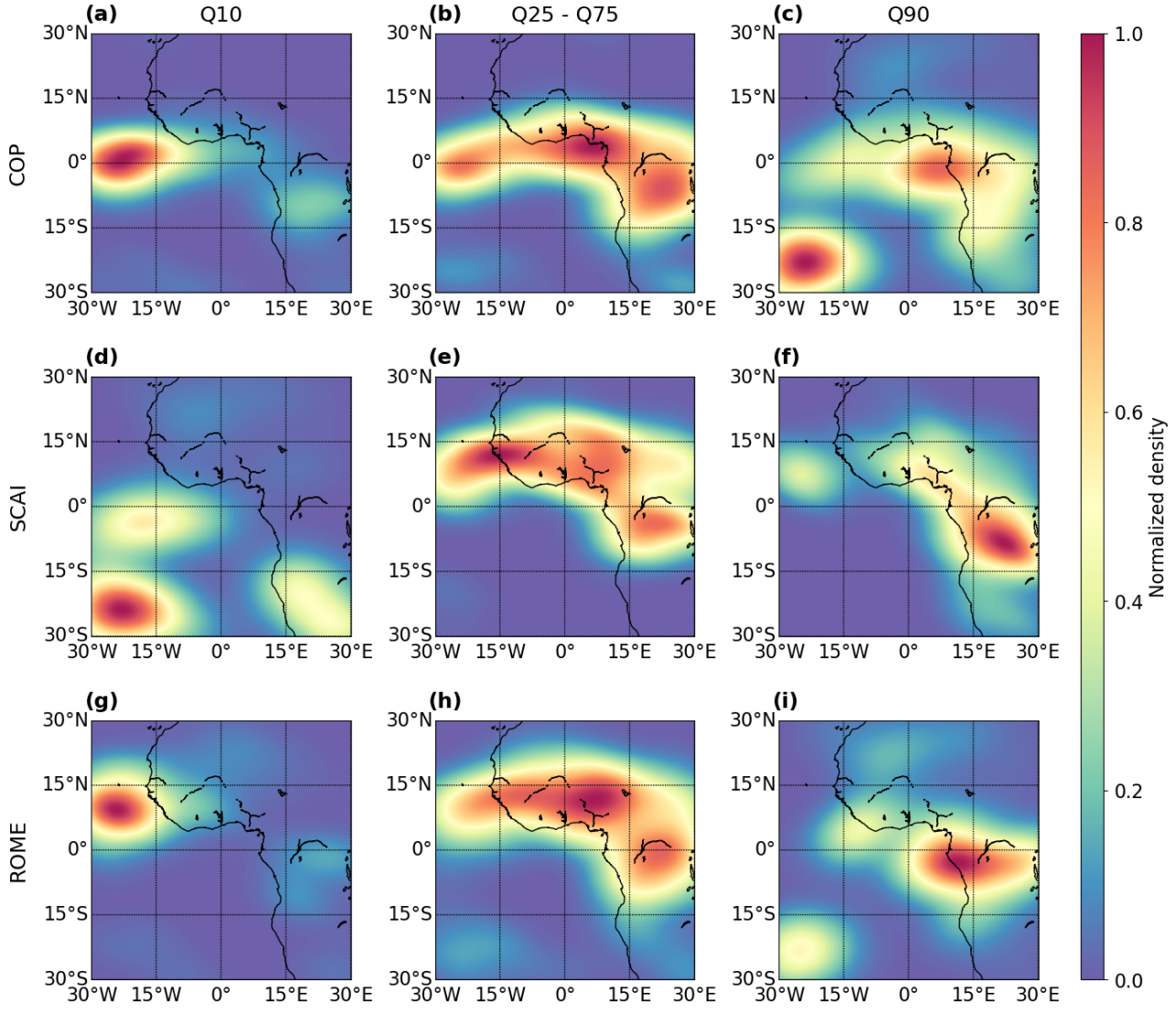

Figure 9. Spatial distribution of convective organisation indices between March and May (MAM) for the COP, SCAI, and ROME. Data points are interpolated on a 3° x 3° grid. Clouds are grouped as strong or weak organised using the **(a,d,g)** 10th (P10), **(b,e,h)** 25th–75th (IQR), **(c,f,i)** 90th (P90) percentile. The values represent the normalized density for each distribution.

https://doi.org/10.5194/egusphere-2025-376
Preprint. Discussion started: 5 February 2025

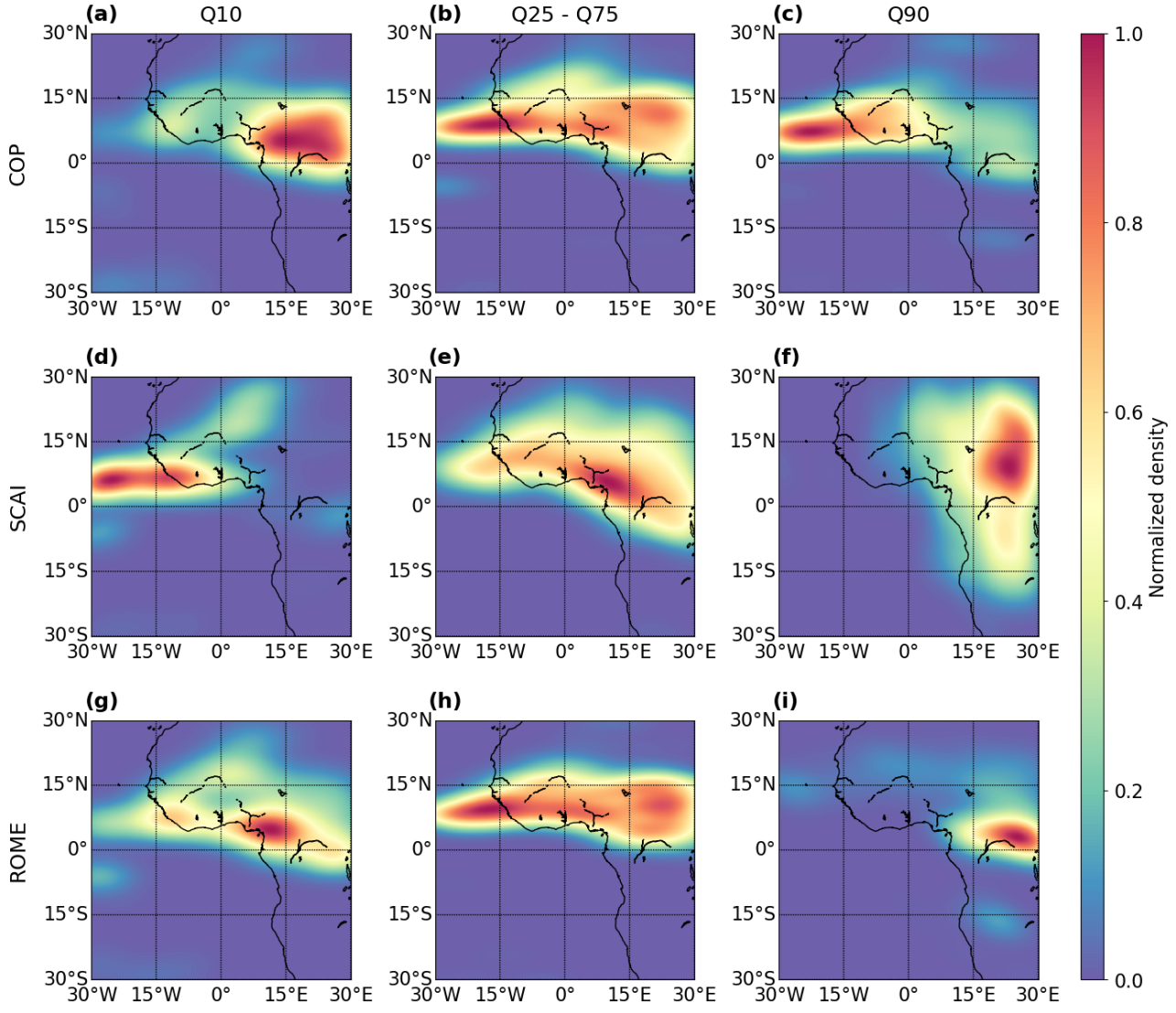

Figure 10. Spatial distribution of convective organisation indices between June and August (JJA) for the COP, SCAI, and ROME. Data points are interpolated on a 3° x 3° grid. Clouds are grouped as strong or weak organised using the **(a,d,g)** 10th (P10), **(b,e,h)** 25th–75th (IQR), **(c,f,i)** 90th (P90) percentile. The values represent the normalized density for each distribution.

https://doi.org/10.5194/egusphere-2025-376
Preprint. Discussion started: 5 February 2025

We combine the percentile locations of the indices (P90, P10) to assess the aggregated distribution of organisation in spring (MAM) and summer (JJA). Averaged over the AOI, a high degree of convective organisation occurs most frequently between 15° S and 15° N. Over the ocean, convective organisation is higher during spring in the southern hemisphere and summer in the northern hemisphere. Over land, it is stronger over the northern hemisphere in summer. Our findings suggest that convective organisation is connected to vertical and horizontal cloud and core properties. A higher degree of organisation comes along an intense convective activity, a larger anvil area, a longer lifetime, and a lower area ratio (Section 4.2.1). In spring, organised cloud systems primarily appear over the Atlantic Ocean and coastal Africa in the southern hemisphere. A second peak reflects the occurrence of oceanic MCSs between 15–30° S (Figure 11, a). We find the weakest organisation over the rainforest and the Atlantic Ocean near the equator (Figure 11, b). In summer, the hotspot locations shift northward. Then, we observe the highest number of organised clouds over the tropical Atlantic Ocean between 0°–15° N. A second peak persists over continental West Africa, the Jos Plateau, and the Congo River.

Along the AOI, the concurrent existence of weakly organised or isolated clouds and highly clustered cloud systems induces hotspots of weak and strong convective organisation that occur in the same area (Figure 5, a–d). They may balance each other out, blurring derived spatio-temporal statistics. The location of this superimposition changes with the season. As shown in Sect. 4.2.1, convective activity is marked by a high variability, especially over oceanic regions. Moreover, we find ambiguous results regarding convective organisation for different hemispheres, surface types, and seasons. These variations may be due to seasonal effects such as the northward shift of the ITCZ (Futyan and Genio, 2007; Atiah et al., 2023). As shown in Part 1 of this study (Brüning and Tost, 2025), regional effects may alter the convective life-cycle. Although we observe a slightly stronger average organisation over the sea (Figure 4), the analysis points out the complexity of deriving distinct patterns of convective organisation.

4.3 Seasonal effects on convective organisation

The seasonal analysis of the organisation indices emphasises a connection between a pronounced convective organisation, the hemisphere, and the surface type (Figure 12). Between March and August, COP and ROME increase in the northern hemisphere. At the same time, we observe ambiguous results for SCAI, with a slight increase over land and a decrease over the ocean (Figure 12, a–c). Differences between the surface types comprise up to 5 % (COP, ROME) and 10 % (SCAI) of the index scale. Over the southern hemisphere, the indices show a higher variability (Figure 12, d–f). We detect a tendency for stronger organisation in the southern hemisphere accompanied by a higher cloud anvil area, cloud lifetime and enhanced core size but reduced CTH (Figure 7). For COP and ROME, we find an increase between March and May, followed by a minimum in June and a renewed increase between July and August. The values of SCAI show a linear decrease from spring to summer. There is a weak to moderate trend towards higher (COP, ROME) or lower (SCAI) index values during summer in the northern hemisphere. In the southern hemisphere, we see an increase in convective organisation over the ocean and a decrease over land.

In Sect. 4.2, we have detected a high spatial variability that modifies regional convective cloud development and organisation patterns. Further, we investigate seasonal differences for cloud and core properties for strongly (P90) and weakly (P10) organised cloud clusters. Following an overall slight increase of convective organisation in summer (Figure 12), we also see a

https://doi.org/10.5194/egusphere-2025-376
Preprint. Discussion started: 5 February 2025

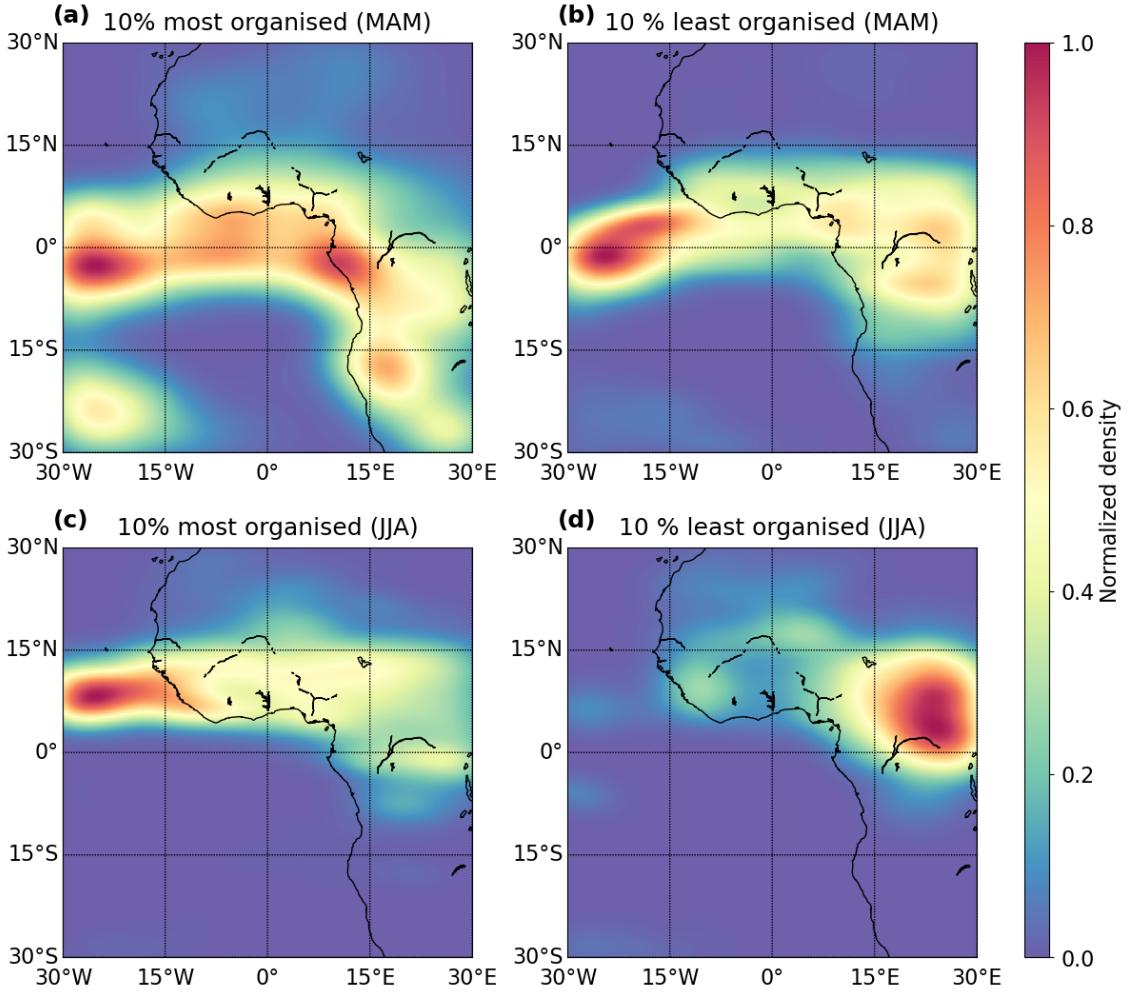

Figure 11. Spatial distribution of convective organisation indices computed by aggregating percentiles of COP, SCAI, and ROME for the months March to May (MAM, upper row) and June to August (JJA, lower row). Clouds are grouped as the **(a) & (c)** most organised or **(b) & (d)** the least organised using the 10 % lowest (SCAI) or highest (COP, ROME) data points. The values represent the normalized density for each distribution interpolated on a 3° x 3° grid.

https://doi.org/10.5194/egusphere-2025-376
Preprint. Discussion started: 5 February 2025

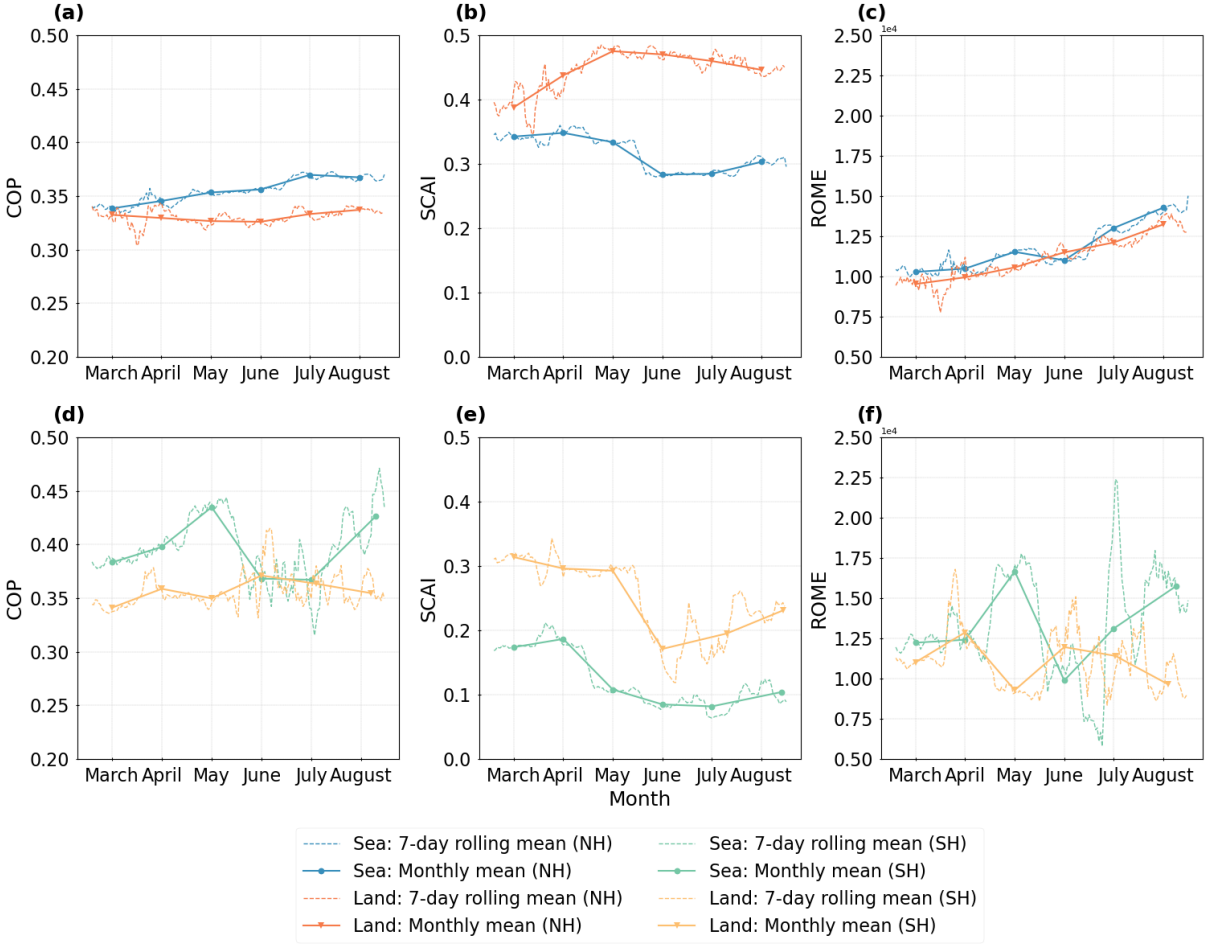

Figure 12. Seasonal changes of the organisation indices in the AOI between March and August 2019 grouped by the hemisphere. We show **(a,d)** the COP, **(b,e)** the SCAI, and **(c,f)** the ROME on the northern (NH, upper row) and southern (SH, lower row) hemisphere over land and sea. We visualise the monthly mean (solid lines) and the 7-day rolling mean (dashed lines).

https://doi.org/10.5194/egusphere-2025-376
Preprint. Discussion started: 5 February 2025

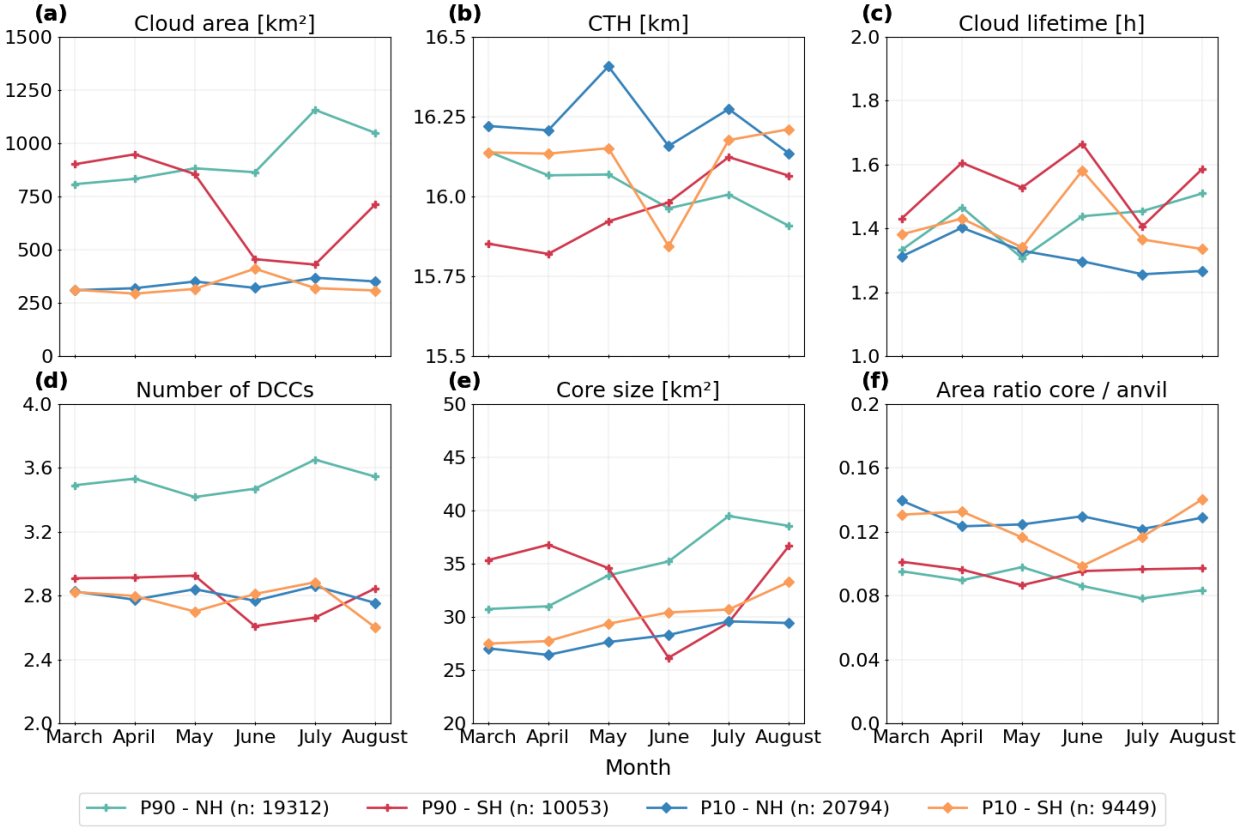

Figure 13. Seasonal changes of the convective cloud and core properties between March and August 2019 grouped by the hemisphere. We see the monthly mean for the 90th (P90, n = 29 365) and 10th (P10, n = 30 243) percentile of **(a)** the cloud anvil area, **(b)** the CTH, **(c)** the cloud lifetime, **(d)** the number of DCCs, **(e)** the convective core area, and **(f)** the area ratio between cloud anvil and core area on the northern (NH) and southern (SH) hemisphere.

weak trend towards more and larger DCCs (Figure 13). Overall, organised clouds (P90) come along a larger cloud anvil area, a longer cloud lifetime, a lower CTH, a lower area ratio, and more and larger DCCs. This pattern appears mainly in the northern hemisphere during summer. However, there is a high spatial variability (Section 4.2). For example, in summer, we observe extensive, long-lasting, and more clustered clouds north of the equator (< 15° N). At the same time, convective activity decreases over the Sahel (> 15° N) (Figure 7). Strong and weak convective organisation is more similar in the southern hemisphere than in the northern hemisphere. Here, we see a weak trend towards smaller and less clustered clouds in the 90th percentile. For weakly organised clouds (P10), we detect more ambiguous results in both hemispheres. These clouds come with a decrease in the cloud lifetime and the number of associated DCCs in summer, whereas the DCC size and CTH increase.

In the following section, we examine the statistical significance of the seasonal differences for organised cloud clusters (P90). For this purpose, we divide the 29 365 cloud clusters into four groups based on the surface type (Sea, Land) and the season

https://doi.org/10.5194/egusphere-2025-376
Preprint. Discussion started: 5 February 2025

(MAM, JJA). The group sizes in our study are imbalanced since more clouds occur over the ocean (Brüning and Tost, 2025). To detect statistically significant differences between the group mean values, we apply Welch's t-test for independent samples. In contrast to the Student's t-test, the results remain robust for skewed distributions and large or uneven sample sizes (Derrick and White, 2016). Moreover, we calculate Cohen's D to complement the t-test results. It measures the difference between two means based on standard deviation units (effect size). Large values of Cohen's D indicate the difference between the means is higher than the variability (Cohen, 2013). The effect size is positive and ranges between 0 and infinity, with a classification indicating small (< 0.2), medium (0.2–0.5), or large (≥ 0.8) differences.

We see an overall shift of the indices' distribution towards a stronger organisation during summer (JJA) (Figure 12, 14 a–c). For COP, we find the highest effect size between oceanic and continental surfaces in summer and the lowest in spring. The seasonal differences are generally higher over land than the ocean. Although the p-values point out statistically significant differences between the means of the distribution, we detect a predominately small effect size. For SCAI, we find higher values and a larger effect size in summer (JJA) (Figure 12). Although the arithmetic mean of SCAI is similar over both surface types, the IQR shows a broader value range over land (Figure 14, a–c). The effect size for ROME is, on average, higher than for COP and SCAI. Again, the distribution shifts towards higher averages in summer. Our analysis emphasises the importance of seasonal and spatial effects on cloud organisation. For instance, we detect statistically significant differences between organised convection in spring (MAM) and summer (JJA) over land and sea ($p < 0.05$). The distributions of COP and ROME show a noticeable narrowing in summer (JJA). However, the effect size suggests the differences are relatively small, except for ROME and SCAI over land.

The distribution of the cloud area, the cloud lifetime, and the core size slightly shift in summer. We observe a broadening over the ocean and a narrowing over land, whereas the median remains similar (Figure 14, d, f, h). Following, we observe only a small effect size. The seasonal variability of the CTH is weaker, particularly over the ocean. Contrasting, we observe higher values of the CTH in summer (JJA). Accordingly, the effect size between the groups over land and sea is enhanced. We find a similar seasonal pattern for the number of DCCs and the area ratio (Figure 14, g, i). However, the effect sizes remain small and suggest only a weaker seasonality for the number of DCCs and the area ratio.

To summarise, the frequency of convective activity and, for instance, the strength of convective organisation increases in the northern hemisphere from spring to summer. In contrast, convective organisation in the southern hemisphere is more pronounced in spring. Compared to the northern hemisphere, the properties of convective clouds and cores are more similar for strong and weak convective organisation. Overall, the southern hemisphere has a higher variability concerning the organisation indices and the frequency of intense convective activity. Regions with different degrees of convective organisation show partly ambiguous results for the associated cloud properties, especially for the core size and CTH. While we find statistically significant differences between organised convection based on spatial and temporal factors, the strength of these effects is predominately small. The derived differences in the distributions may not be sufficient to explain the spatio-temporal variability of the patterns we detected in Sect. 4.2. However, the total of detected uncertainties and limitations reflect the complexity in quantifying convective organisation.

https://doi.org/10.5194/egusphere-2025-376
Preprint. Discussion started: 5 February 2025

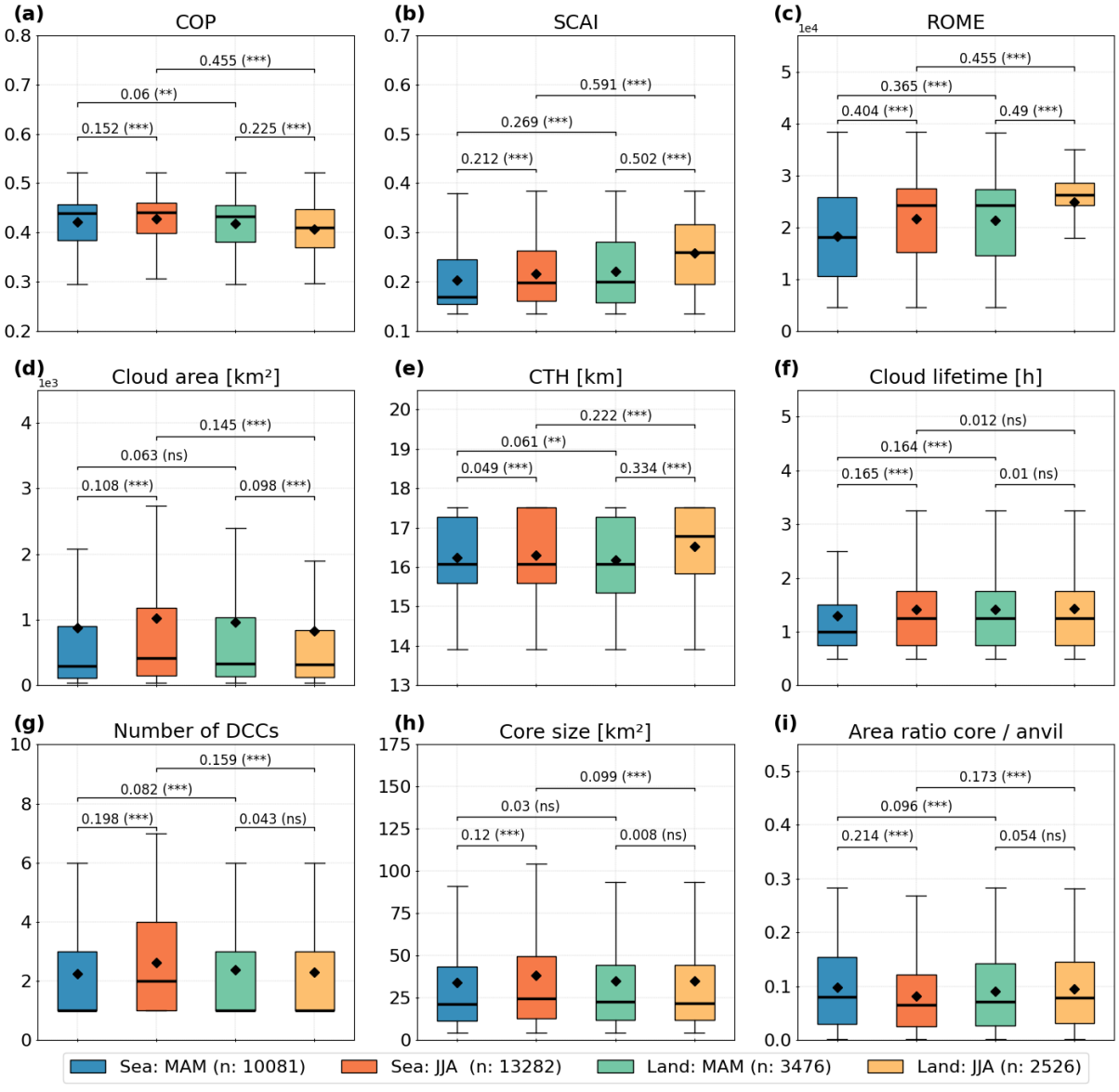

Figure 14. Boxplot for organised cloud clusters (P90, n = 29 365) grouped by the surface type (Sea, Land) and season (MAM, JJA). We show **(a)** the COP, **(b)** the SCAI, **(c)** the ROME, **(d)** the cloud anvil area, **(e)** the CTH, **(f)** the cloud lifetime, **(g)** the number of DCCs, **(h)** the convective core area, and **(i)** the area ratio between cloud anvil and core area. The boxplot contains the median (bold black lines) and the arithmetic mean (black diamonds). Annotations depict the effect size measured by Cohen's D and the p-value derived from Welch's t-test (not significant (ns): $p \geq 0.1$, significant with *: $p < 0.1$, **: $p < 0.05$, ***: $p < 0.01$).

https://doi.org/10.5194/egusphere-2025-376
Preprint. Discussion started: 5 February 2025

5 Discussion

According to results by Stubenrauch et al. (2023), strong convective organisation is associated with larger, more clustered convective systems (Section 4.1). We find a connection between the spatio-temporal variability of convective organisation and the microphysical cloud properties such as the cloud anvil area, the CTH, or the cloud lifetime (Bläckberg and Singh, 2022). In our study, organisation indices vary with the cluster size, cloud lifetime, and the ratio between the DCCs and the anvil area (Section 4.1, 4.2.1). MCSs with a lower area ratio appear as more organised (Section 4.2.2). Within clustered clouds like MCSs, interactions between DCCs may enhance the convective activity and prolong the cloud lifetime, anvil growth, and vertical updraft strength (Tompkins and Semie, 2017). In contrast to previous results (Takahashi et al., 2017; Stubenrauch et al., 2023), we detect a slightly stronger organisation over the ocean, which may be due to the dominance of oceanic clouds in our study (Section 4.1). Moreover, the results may reflect an extensive transport of continental convective clusters towards the ocean (Vondou, 2012). The differences over land and sea account for about 10 %, which is lower than the seasonal difference of about 15–20 %. A higher seasonal variability of convective activity in the southern hemisphere is associated to a more fluctuating strength of organisation. However, the microphysical properties of weakly and strongly organised clouds are more similar than in the northern hemisphere. For continental cloud clusters in the northern hemisphere, we find more distinct results regarding the relationship between DCCs and the degree of organisation (Section 4.2.2). Our results show that grouping organised cloud clusters by temporal and spatial factors like the season or surface type reveals statistically significant differences ($p < 0.05$) between the means of their distribution (Section 4.2.2). Nevertheless, the absolute difference for the convective cloud properties between these groups remains predominately small. Contrasting, we find a higher variability and a medium to high effect size for the organisation indices (Section 4.3). While the analysis helps to assess spatio-temporal patterns of convective organisation, further advancing the understanding of underlying processes may require the integration of additional properties. Moreover, a less skewed distribution for clouds over land and ocean may reduce the imbalance between group sizes and improve the robustness of statistics.

Our results emphasise that changes on multiple scales influence convective cloud organisation. When comparing spatial patterns, we see ambiguous results for organisation indices in the southern and northern hemispheres and between regions near the equator and the tropics (Section 4.2). Convective organisation may be driven by the interplay of processes induced by, e.g., local surface characteristics (Vondou, 2012), the monsoon circulation (Futyan and Genio, 2007), or the katabatic flow in mountainous regions (Nicholson, 2018). Narrowing down their effect on convective organisation requires further clarification. Moreover, we detect overlapping effects of weak and strong organisation that blur the statistical analysis (Section 4.2.2). The currently employed indices allow us to identify geographical patterns of large-scale cloud clustering. Nevertheless, further uncertainties persist. These comprise the impact of the terrain on cloud organisation and its connection to severe weather (Biagioli and Tompkins, 2023). A metric built simultaneously using more indices or integrating spatial and temporal factors in the calculation may enhance the results (Pscheidt et al., 2019). This study employs a grid-based approach with a moving window (Section 3.2). Before, numerous studies applied the idea of partitioning the AOI into subsets of an equal area (e.g., Tobin et al. (2012); Stubenrauch et al. (2023); Retsch et al. (2020)). While a moving window may prevent small-scale fluctuations between

https://doi.org/10.5194/egusphere-2025-376
Preprint. Discussion started: 5 February 2025

grid cells, it is still based on a somewhat arbitrary, human-induced split. In contrast, unsupervised clustering algorithms like DBSCAN or the improved HDBSCAN may provide a more data-driven approach. Zuo et al. (2022) used the DBSCAN algorithm to identify cloud clusters within 3D radar data. Furthermore, Kim et al. (2023) derived precipitation probabilities from geostationary satellite data with an unsupervised clustering technique. In our following work, we will investigate whether these algorithms are suitable to identify robust patterns of convective cloud organisation through space and time.

5.1 Spatio-temporal drivers of organisation

Referring to our findings from Part 1 of this paper sequence (Brüning and Tost, 2025), convective cloud development is subject to spatial and temporal changes. These effects come into play regionally and on a larger scale. We see a link between intense convective cores, extensive MCSs and the occurrence of convective organisation. In spring, we observe a weaker convective activity represented by smaller cloud anvils and fewer and smaller convective cores. In summer, increasing core sizes emphasise that convective activity is enhanced over land and sea (Takahashi et al., 2023). Strong organisation occurs in spring (southern hemisphere) and summer (northern hemisphere), especially during the afternoon over land and at night over the ocean. The diurnal cycle of the organisation indices implies a shift compared to a maximum of convective development (Li et al., 2021). We see a regional peak in organisation over the Atlantic Ocean and coastal West Africa. Organised clouds with larger cores and a prolonged life-cycle appear primarily in the vicinity of the Gulf of Guinea and secondarily in coastal and rainforest regions of continental Africa (Section 4.2). Over the tropical Atlantic Ocean, we find lower cloud tops and warmer MCSs, but also high values of ROME and COP. We emphasise that organisation is not only affected by convective intensity (Takahashi et al., 2017). Instead, extra-tropical MCSs may act as additional drivers for convective organisation (Futyan and Genio, 2007). In the southern hemisphere, we find a high variability for convective development and spatio-temporal patterns of organisation. Here, regional circulations and the continental landmass distribution may alter the annual cycle of cloud development, affecting our results (Brune et al., 2020).

5.2 The role of the ITCZ on large-scale organisation

We observe a connection between DCCs and spatial patterns of convective organisation following the northward propagation of the ITCZ in summer (Figure 10, 11). The WAM links to the Hadley circulation. As a result, the tropical rain belt over West Africa and the Sahel rainfall are subject to seasonal changes (Jackson et al., 2022). The ITCZ drives the tropospheric circulation (Vondou, 2012). Its seasonal shift affects the microphysical cloud properties through its influence on surface characteristics, solar radiation and the local circulation (Kniffka et al., 2019). The ITCZ brings greater humidity in the northern Sahel and the Sahara in summer. Following, we observe a weaker subtropical subsidence rate over the Sahara and a deeper ascent within the tropical rain belt (Fontaine and Philippon, 2000). The seasonal meridional pressure gradients strengthen the low-level moisture transport across adjacent regions (Lavaysse et al., 2009) and may lead to the observed promotion of convective activity in the northern hemisphere (Section 4.3). This seasonality is reflected in our results by an increase of more intense, larger DCCs, larger cloud anvils, and an enhanced degree of convective organisation between June and August (Section 4.2.2). Although the role of the ITCZ as a prolific producer of rainfall has been studied before, the correlation between organisation and heavy rain

https://doi.org/10.5194/egusphere-2025-376
Preprint. Discussion started: 5 February 2025

requires further investigation (Bao et al., 2024). Analysing an extended time series may offer a more detailed perspective on the annual cycle of convective organisation (Takahashi et al., 2017). Furthermore, it may benefit the accuracy and timeliness of operational forecasts and early-warning systems (Pendergrass, 2020).

6 Conclusions

This study investigates spatio-temporal patterns of convective organisation in tropical West Africa using ML-based 3D radar reflectivities. For this purpose, we employ three organisation indices to identify and statistically analyse regional hotspots of convective organisation. Along the AOI, we find the strongest convective organisation in the Atlantic Ocean of the southern hemisphere and the coastal regions of West Africa. The convective activity diverges in regions near the tropics and the equator. Around the equator, we observe concurrent hotspots of weak and strong convective organisation in the same region. They superimpose each other, blurring spatial statistics. Overall, the strength of organisation is connected not only to the cluster size and lifetime but also to the number and size of DCCs within a cluster. We detect an increase in convective organisation especially for systems with more than 10 DCCs. While our results agree with previous research, we observe that convective organisation is about 5–10 % stronger over the ocean. However, seasonal and zonal effects account for 10–20 % of the organisation index scale. The seasonal analysis of the percentile locations emphasises a connection between convective clustering and large-scale forcings, such as the shift of the ITCZ. The employed indices show partly ambiguous results. These uncertainties reflect the specific limitations of each index. Current indices cannot sufficiently characterise the degree of convective organisation. Here, ROME shows the highest agreement to previous findings suggesting a a stronger convective organisation over land. Nevertheless, all indices are subject to spatio-temporal variations. Including this variability in an adapted index may benefit the accuracy of the results. In summary, our study emphasises the need to quantify the mechanisms that control convective organisation on a regional level. An in-depth understanding is necessary to improve the representation of convective clouds and enhance a future climate risk assessment.

Appendix A: Impact of the hemisphere on seasonal differences of organised convection

We complement our findings from Sect. 4.2 and Sect. 4.3 by evaluating whether seasonal differences of organised convection along the hemispheres are statistically significant (Figure A1). The differences between the northern (NH) and southern (SH) hemispheres generally agree with the results described in Sect. 4.3. We observe statistically significant differences between the groups regarding the organisation indices and parts of the cloud properties ($p < 0.05$). However, the effect sizes are predominantly small, particularly for the cloud properties (Figure A1, d–i). The results emphasise convective organisation increases in summer (JJA) (Figure A1, a–c). For instance, the effect size is higher between the two hemispheres than the seasons (COP, SCAI). Except for the CTH, the distributions of all cloud parameters shift towards a higher mean in NH summer. In the southern hemisphere, the seasonal differences are minor or even reversed. This finding reinforces the assumption of a seasonally opposed pattern for organised convection in the southern and northern hemispheres.

https://doi.org/10.5194/egusphere-2025-376
Preprint. Discussion started: 5 February 2025

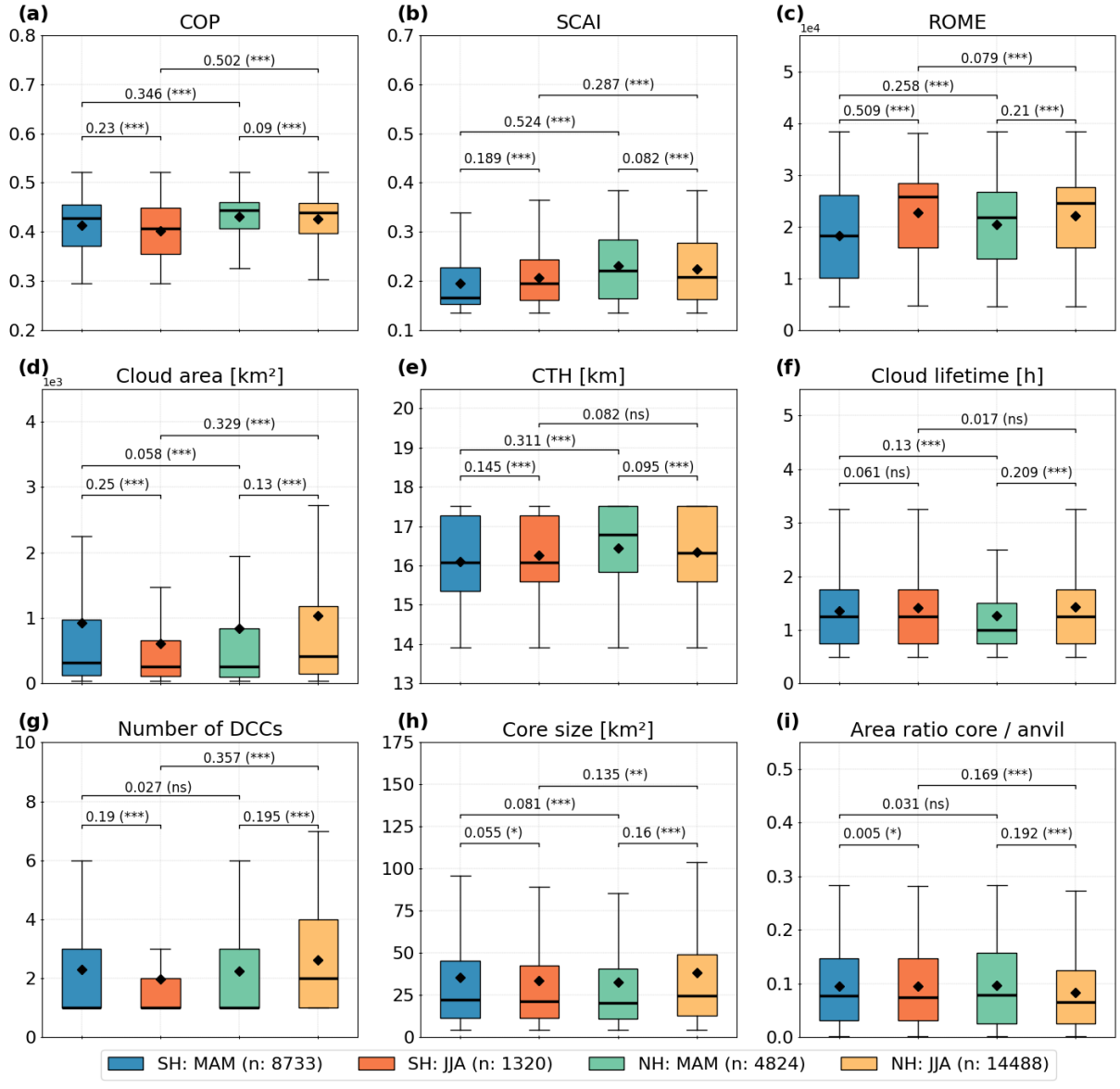

Figure A1. Boxplot for organised cloud clusters (P90, n = 29 365) grouped by the hemisphere (NH, SH) and season (MAM, JJA). We show **(a)** the COP, **(b)** the SCAI, **(c)** the ROME, **(d)** the cloud anvil area, **(e)** the CTH, **(f)** the cloud lifetime, **(g)** the number of DCCs, **(h)** the convective core area, and **(i)** the area ratio between cloud anvil and core area. The boxplot contains the median (bold black lines) and the arithmetic mean (black diamonds). Annotations depict the effect size measured by Cohen's D and the p-value derived from Welch's t-test (not significant (ns): $p \geq 0.1$, significant with *: $p < 0.1$, **: $p < 0.05$, ***: $p < 0.01$).

https://doi.org/10.5194/egusphere-2025-376
Preprint. Discussion started: 5 February 2025

Code and data availability. The level 2B-GEOPROF CloudSat data used in this study are available at the CloudSat Data Processing Center at CIRA/Colorado State University and can be retrieved from http://www.CloudSat.cira.colostate.edu/order-data (CloudSat Data Processing Center, 2024). The Meteosat SEVIRI level 1.5 data used in this study is freely and openly available via the EUMETSAT Data Store at https://navigator.eumetsat.int/product/EO-:EUM:DAT:MSG:HRSEVIRI (EUMETSAT Data Services, 2024). The code used in this study will be released upon publication.

Author contributions. S.B and H.T. designed the study. S.B developed the code for performing the analysis and visualisation. S.B. and H.T. contributed to analysing and evaluating spatio-temporal patterns of convective cloud organisation. S.B. and H.T. wrote the draft of the paper. All authors have read and agreed to the published version of the manuscript.

Competing interests. The authors declare that they have no conflict of interest.

Acknowledgements. This work was supported by the project "Big Data in Atmospheric Physics (BINARY)", funded by the Carl Zeiss Foundation (grant P2018-02-003), and the Max Planck Graduate Center with the Johannes Gutenberg University of Mainz (MPGC). We thank EUMETSAT for providing access to the Meteosat SEVIRI imager data and the Cooperative Institute for Research in the Atmosphere, CSU, for providing access to the CloudSat 2B-GEOPROF data.

https://doi.org/10.5194/egusphere-2025-376
Preprint. Discussion started: 5 February 2025

References

Atiah, W. A., Amekudzi, L. K., and Danuor, S. K.: Mesoscale convective systems and contributions to flood cases in Southern West Africa (SWA): A systematic review, Weather and Climate Extremes, 39, 100 551, https://doi.org/10.1016/j.wace.2023.100551, 2023.

Bao, J., Stevens, B., Kluft, L., and Muller, C.: Intensification of daily tropical precipitation extremes from more organized convection, Sci. Adv., 10, eadj6801, https://doi.org/10.1126/sciadv.adj6801, 2024.

Becker, T., Bechtold, P., and Sandu, I.: Characteristics of convective precipitation over tropical Africa in storm-resolving global simulations, Q. J. R. Meteorol. Soc., 147, 4388–4407, https://doi.org/10.1002/qj.4185, 2021.

Berthou, S., Rowell, D. P., Kendon, E. J., Roberts, M. J., Stratton, R. A., Crook, J. A., and Wilcox, C.: Improved climatological precipitation characteristics over West Africa at convection-permitting scales, Clim. Dyn., 53, 1991–2011, https://doi.org/10.1007/s00382-019-04759-4, 2019.

Biagioli, G. and Tompkins, A. M.: Measuring Convective Organization, JAS, 80, 2769–2789, https://doi.org/10.1175/JAS-D-23-0103.1, 2023.

Bläckberg, C. P. O. and Singh, M. S.: Increased Large-Scale Convective Aggregation in CMIP5 Projections: Implications for Tropical Precipitation Extremes, Geophys. Res. Lett., 49, e2021GL097 295, https://doi.org/10.1029/2021GL097295, 2022.

Brune, S., Buschow, S., and Friederichs, P.: Observations and high-resolution simulations of convective precipitation organization over the tropical Atlantic, Q. J. R. Meteorol. Soc., 146, 1545–1563, https://doi.org/10.1002/qj.3751, 2020.

Brüning, S. and Tost, H.: A ML-based perspective on deep convective clouds and their organisation in 3D. Part I: Influence of deep convective cores on the cloud life-cycle, submitted to EGUsphere, 2025.

Brüning, S., Niebler, S., and Tost, H.: Artificial intelligence (AI)-derived 3D cloud tomography from geostationary 2D satellite data, Atmos. Meas. Tech., 17, 961–978, https://doi.org/10.5194/amt-17-961-2024, 2024.

Chen, P.-J., Chen, W.-T., Wu, C.-M., and Yo, T.-S.: Convective Cloud Regimes From a Classification of Object-Based CloudSat Observations Over Asian-Australian Monsoon Areas, Geophys. Res. Lett., 48, e2021GL092 733, https://doi.org/10.1029/2021GL092733, 2021.

CloudSat Data Processing Center: Data Products, CloudSat DPC [data set], https://www.cloudsat.cira.colostate.edu/data-products, accessed: 2024-12-12, 2024.

Cohen, J.: Statistical Power Analysis for the Behavioral Sciences, Routledge, 2 edn., https://doi.org/10.4324/9780203771587, 2013.

Coppin, D. and Bony, S.: Physical mechanisms controlling the initiation of convective self-aggregation in a General Circulation Model, J. Adv. Model. Earth Syst., 7, 2060–2078, https://doi.org/10.1002/2015MS000571, 2015.

Cui, W., Dong, X., Xi, B., and Feng, Z.: Climatology of Linear Mesoscale Convective System Morphology in the United States Based on the Random-Forests Method, J. Clim., 34, 7257–7276, https://doi.org/10.1175/JCLI-D-20-0862.1, 2021.

Dauhut, T., Chaboureau, J.-P., Escobar, J., and Mascart, P.: Giga-LES of Hector the Convector and Its Two Tallest Updrafts up to the Stratosphere, JAS, 73, 5041–5060, https://doi.org/10.1175/JAS-D-16-0083.1, 2016.

Derrick, B. and White, P.: Why Welch's test is Type I error robust, TQMP, 12, 30–38, https://doi.org/10.20982/tqmp.12.1.p030, 2016.

EUMETSAT Data Services: High Rate SEVIRI Level 1.5 Image Data - MSG - 0 degree, https://navigator.eumetsat.int/product/EO:EUM:DAT:MSG:HRSEVIRI, accessed: 2024-12-12, 2024.

Feng, Z., Varble, A., Hardin, J., Marquis, J., Hunzinger, A., Zhang, Z., and Thieman, M.: Deep Convection Initiation, Growth, and Environments in the Complex Terrain of Central Argentina during CACTI, Mon. Weather Rev., 150, 1135–1155, https://doi.org/10.1175/MWR-D-21-0237.1, 2022.

https://doi.org/10.5194/egusphere-2025-376
Preprint. Discussion started: 5 February 2025

Fink, A. H., Vincent, D. G., and Ermert, V.: Rainfall Types in the West African Sudanian Zone during the Summer Monsoon 2002, Mon. Weather Rev., 134, 2143–2164, https://doi.org/10.1175/MWR3182.1, 2006.

Fontaine, B. and Philippon, N.: Seasonal evolution of boundary layer heat content in the West African monsoon from the NCEP/NCAR reanalysis (1968–1998), Int. J. Climatol., 20, 1777–1790, https://doi.org/10.1002/1097-0088(20001130)20:14<1777::AID-JOC568>3.0.CO;2-S, 2000.

Futyan, J. M. and Genio, A. D. D.: Deep Convective System Evolution over Africa and the Tropical Atlantic, J. Clim., 20, 5041–5060, https://doi.org/10.1175/JCLI4297.1, 2007.

Haerter, J. O., Böing, S. J., Henneberg, O., and Nissen, S. B.: Circling in on Convective Organization, Geophys. Res. Lett., 46, 7024–7034, https://doi.org/10.1029/2019GL082092, 2019.

Hartmann, D. L., Hendon, H. H., and Houze, R. A.: Some Implications of the Mesoscale Circulations in Tropical Cloud Clusters for Large-Scale Dynamics and Climate, JAS, 41, 113–121, https://doi.org/10.1175/1520-0469(1984)041<0113:SIOTMC>2.0.CO;2, 1984.

Houze, R. A.: Structure and Dynamics of a Tropical Squall–Line System, Mon. Wea. Rev., 105, 1540–1567, https://doi.org/10.1175/1520-0493(1977)105<1540:SADOAT>2.0.CO;2, 1977.

Igel, M. R., Drager, A. J., and van den Heever, S. C.: A CloudSat Cloud-Object Partitioning Technique and Assessment and Integration of Deep Convective Anvil Sensitivities to Sea Surface Temperature, J. Geophys. Res. Atmos., 119, 10 515–10 535, https://doi.org/10.1002/2014JD021717, 2014.

Jackson, L. S., Marsham, J. H., Parker, D. J., Finney, D. L., Fitzpatrick, R. G. J., Rowell, D. P., Stratton, R. A., and Tucker, S.: The Effect of Explicit Convection on Climate Change in the West African Monsoon and Central West African Sahel Rainfall, J. Clim., 35, 1537–1557, https://doi.org/10.1175/JCLI-D-21-0258.1, 2022.

Jin, D., Oreopoulos, L., Lee, D., Tan, J., and Kim, K.-m.: A New Organization Metric for Synoptic Scale Tropical Convective Aggregation, J. Geophys. Res. Atmos., 127, e2022JD036 665, https://doi.org/10.1029/2022JD036665, 2022.

Jones, W., Christensen, M., and Stier, P.: A semi-Lagrangian method for detecting and tracking deep convective clouds in geostationary satellite observations, Atmos. Meas. Tech., 16, 1043–1059, https://doi.org/10.5194/amt-16-1043-2023, 2023.

Jones, W., Stengel, M., and Stier, P.: A Lagrangian perspective on the lifecycle and cloud radiative effect of deep convective clouds over Africa, Atmos. Chem. Phys., 24, 5165–5180, https://doi.org/10.5194/acp-24-5165-2024, 2024.

Kim, D., Kim, H.-J., and Choi, Y.-S.: Unsupervised Clustering of Geostationary Satellite Cloud Properties for Estimating Precipitation Probabilities of Tropical Convective Clouds, J. Appl. Meteorol., 62, 1083–1094, https://doi.org/10.1175/JAMC-D-22-0175.1, 2023.

Klein, C., Nkrumah, F., Taylor, C. M., and Adefisan, E. A.: Seasonality and Trends of Drivers of Mesoscale Convective Systems in Southern West Africa, J. Clim., 34, 71–87, https://doi.org/10.1175/JCLI-D-20-0194.1, 2021.

Kniffka, A., Knippertz, P., and Fink, A. H.: The role of low-level clouds in the West African monsoon system, Atmos. Chem. Phys., 19, 1623–1647, https://doi.org/10.5194/acp-19-1623-2019, 2019.

Lavaysse, C., Flamant, C., Janicot, S., Parker, D. J., Lafore, J.-P., Sultan, B., and Pelon, J.: Seasonal evolution of the West African heat low: a climatological perspective, Clim Dyn, 33, 313–330, https://doi.org/10.1007/s00382-009-0553-4, 2009.

Li, W., Zhang, F., Yu, Y., Iwabuchi, H., Shen, Z., Wang, G., and Zhang, Y.: The semi-diurnal cycle of deep convective systems over Eastern China and its surrounding seas in summer based on an automatic tracking algorithm, Clim. Dyn., 56, 357–379, https://doi.org/10.1007/s00382-020-05474-1, 2021.

Mandorli, G. and Stubenrauch, C. J.: Assessment of object-based indices to identify convective organization, Geosci. Model Dev., 17, 7795–7813, https://doi.org/10.5194/gmd-17-7795-2024, 2024.

https://doi.org/10.5194/egusphere-2025-376
Preprint. Discussion started: 5 February 2025

Muller, C. and Bony, S.: What favors convective aggregation and why?, Geophys. Res. Lett., 42, 5626–5634, https://doi.org/10.1002/2015GL064260, 2015.

Nicholson, S. E.: The ITCZ and the Seasonal Cycle over Equatorial Africa, BAMS, 99, 337–348, https://doi.org/10.1175/BAMS-D-16-0287.1, 2018.

Pendergrass, A. G.: Changing Degree of Convective Organization as a Mechanism for Dynamic Changes in Extreme Precipitation, Curr. Clim. Change Rep., 6, 47–54, https://doi.org/10.1007/s40641-020-00157-9, 2020.

Pscheidt, I., Senf, F., Heinze, R., Deneke, H., Trömel, S., and Hohenegger, C.: How organized is deep convection over Germany?, Q. J. R. Meteorol. Soc., 145, 2366–2384, https://doi.org/10.1002/qj.3552, 2019.

Rempel, M., Senf, F., and Deneke, H.: Object-Based Metrics for Forecast Verification of Convective Development with Geostationary Satellite Data, Mon. Wea. Rev., 145, 3161–3178, https://doi.org/10.1175/MWR-D-16-0480.1, 2017.

Retsch, M. H., Jakob, C., and Singh, M. S.: Assessing Convective Organization in Tropical Radar Observations, J. Geophys. Res. Atmos., 125, e2019JD031 801, https://doi.org/10.1029/2019JD031801, 2020.

Ronneberger, O., Fischer, P., and Brox, T.: U-Net: Convolutional Networks for Biomedical Image Segmentation, in: Medical Image Computing and Computer-Assisted Intervention – MICCAI 2015, edited by Navab, N., Hornegger, J., Wells, W. M., and Frangi, A. F., vol. 9351, pp. 234–241, Springer International Publishing, Cham, 2015.

Schmetz, J., Pili, P., Tjemkes, S., Just, D., Kerkmann, J., Rota, S., and Ratier, A.: An introduction to Metetsat second generation (MSG), BAMS, 83, 977–992, https://doi.org/10.1175/1520-0477(2002)083<0977:AITMSG>2.3.CO;2, 2002.

Semie, A. G. and Bony, S.: Relationship Between Precipitation Extremes and Convective Organization Inferred From Satellite Observations, Geophys. Res. Lett., 47, e2019GL086 927, https://doi.org/10.1029/2019GL086927, 2020.

Sokolowsky, G. A., Freeman, S. W., Jones, W. K., Kukulies, J., Senf, F., Marinescu, P. J., Heikenfeld, M., Brunner, K. N., Bruning, E. C., Collis, S. M., Jackson, R. C., Leung, G. R., Pfeifer, N., Raut, B. A., Saleeby, S. M., Stier, P., and van den Heever, S. C.: *tobac* v1.5: introducing fast 3D tracking, splits and mergers, and other enhancements for identifying and analysing meteorological phenomena, Geosci. Model Dev., 17, 5309–5330, https://doi.org/10.5194/gmd-17-5309-2024, 2024.

Stephens, G. L., Vane, D. G., Tanelli, S., Im, E., Durden, S., Rokey, M., Reinke, D., Partain, P., Mace, G. G., Austin, R., L'Ecuyer, T., Haynes, J., Lebsock, M., Suzuki, K., Waliser, D., Wu, D., Kay, J., Gettelman, A., Wang, Z., and Marchand, R.: CloudSat mission: Performance and early science after the first year of operation, J. Geophys. Res. Atmos., 113, https://doi.org/10.1029/2008JD009982, 2008.

Stubenrauch, C. J., Mandorli, G., and Lemaitre, E.: Convective organization and 3D structure of tropical cloud systems deduced from synergistic A-Train observations and machine learning, Atmos. Chem. Phys., 23, 5867–5884, https://doi.org/10.5194/acp-23-5867-2023, 2023.

Takahashi, H., Luo, Z. J., and Stephens, G. L.: Level of neutral buoyancy, deep convective outflow, and convective core: New perspectives based on 5 years of CloudSat data, J. Geophys. Res. Atmos., 122, 2958–2969, https://doi.org/10.1002/2016JD025969, 2017.

Takahashi, H., Luo, Z. J., Stephens, G., and Mulholland, J. P.: Revisiting the Land-Ocean Contrasts in Deep Convective Cloud Intensity Using Global Satellite Observations, Geophys. Res. Lett., 50, e2022GL102 089, https://doi.org/10.1029/2022GL102089, 2023.

Tan, J., Jakob, C., Rossow, W. B., and Tselioudis, G.: Increases in tropical rainfall driven by changes in frequency of organized deep convection, Nature, 519, 451–454, https://doi.org/10.1038/nature14339, 2015.

Taylor, C. M., Klein, C., Dione, C., Parker, D. J., Marsham, J., Diop, C. A., Fletcher, J., Chaibou, A. A. S., Nafissa, D. B., Semeena, V. S., Cole, S. J., and Anderson, S. R.: Nowcasting tracks of severe convective storms in West Africa from observations of land surface state, Environ. Res. Lett., 17, 034 016, https://doi.org/10.1088/1748-9326/ac536d, 2022.

https://doi.org/10.5194/egusphere-2025-376
Preprint. Discussion started: 5 February 2025

Tobin, I., Bony, S., and Roca, R.: Observational Evidence for Relationships between the Degree of Aggregation of Deep Convection, Water Vapor, Surface Fluxes, and Radiation, J. Clim., 25, 6885–6904, https://doi.org/10.1175/JCLI-D-11-00258.1, 2012.

Tompkins, A. M. and Semie, A. G.: Organization of tropical convection in low vertical wind shears: Role of updraft entrainment, J. Adv. Model. Earth Syst., 9, 1046–1068, https://doi.org/10.1002/2016MS000802, 2017.

Vondou, D. A.: Spatio-Temporal Variability of Western Central African Convection from Infrared Observations, Atmos., 3, 377–399, https://doi.org/10.3390/atmos3030377, 2012.

White, B. A., Buchanan, A. M., Birch, C. E., Stier, P., and Pearson, K. J.: Quantifying the Effects of Horizontal Grid Length and Parameterized Convection on the Degree of Convective Organization Using a Metric of the Potential for Convective Interaction, JAS, 75, 425–450, https://doi.org/10.1175/JAS-D-16-0307.1, 2018.

Wing, A. A. and Emanuel, K. A.: Physical mechanisms controlling self-aggregation of convection in idealized numerical modeling simulations, JAMES, 6, 59–74, https://doi.org/10.1002/2013MS000269, 2014.

Wing, A. A., Emanuel, K., Holloway, C. E., and Muller, C.: Convective Self-Aggregation in Numerical Simulations: A Review, Surv Geophys, 38, 1173–1197, https://doi.org/10.1007/s10712-017-9408-4, 2017.

Zipser, E. J., Cecil, D. J., Liu, C., Nesbitt, S. W., and Yorty, D. P.: Where are the most intense thunderstorms on earth?, BAMS, 87, 1057–1072, https://doi.org/10.1175/BAMS-87-8-1057, 2006.

Zuo, Y., Hu, Z., Yuan, S., Zheng, J., Yin, X., and Li, B.: Identification of Convective and Stratiform Clouds Based on the Improved DBSCAN Clustering Algorithm, Adv. Atmos. Sci., 39, 2203–2212, https://doi.org/10.1007/s00376-021-1223-7, 2022.